# MULTISCALE MODELS OF METALLIC PARTICLES IN NEMATIC LIQUID CRYSTALS*

THOMAS P. BENNETT†, GIAMPAOLO D'ALESSANDRO†, AND KEITH R. DALY‡

**Abstract.** In this paper we use the method of homogenization to derive a set of approximate equations which describe a nematic liquid crystal colloid in which the dopants are freely rotating metallic particles. Previously we have studied the approximate behavior of liquid crystals doped with particles under the assumption that these remain stationary [6]. This paper builds on [6] by extending the theory to include rotating particles. We find a set of governing equations for the nematic liquid crystal and for the dopant particles. Effective material parameters are given explicitly in terms of the microscopic particle-liquid crystal interaction parameters by a sequence of cell problems solved on the micro-scale. We validate our model by direct comparison to large scale numerical simulation and find excellent agreement for a variety of dopants shapes.

**Key words.** Homogenization, nematic liquid crystals, colloidal suspensions, approximation methods, numerical methods

**AMS subject classifications.** 35B27, 76A15, 35Q35, 82D30

**1. Introduction.** Colloidal nematic systems consist of micro- to nanometer sized dopant particles suspended in a nematic liquid crystal. They have been studied either as models for self-assembly of two and three dimensional structures [30, 18, 12, 41] or as a tool to enhance the liquid crystal linear [24] and nonlinear [22, 21, 48] properties. The particles disrupt the nematic alignment and cause elastic distortions whose nature depends on the strength of the anchoring of the liquid crystal molecules on the particle surface. In the strong anchoring limit defects can form near the particles and are tethered to them. In these cases it is often the interaction of a small number of particles that is of interest [20, 17, 49]. Typical research topics include stability of different director configurations [46] and particle self-assembly through long range elastic interactions [3, 40].

In this paper we are primarily interested in the weak anchoring regime, a regime characterized by low anchoring energy or small particle size. As a consequence, defects are not present [39]: the liquid crystal alignment is distorted by the presence of the particles, but the scalar order parameter remains approximately constant. Such colloidal suspension are optically homogeneous and, hence, of interest to devices and light-based applications. The net effect of the dopants is to alter the material properties of the nematic resulting in a new composite material with enhanced interaction with externally applied electromagnetic fields [22]. In particular, gold nanoparticles suspended in liquid crystals [21], the main example used in this paper, lower their nematic–isotropic transition temperature [34], increase their switching speed [28], introduce tunability of their dielectric anisotropy [36] and increase considerably their thermal nonlinearity [32] which, in addition, can also be tuned using an external voltage [25]. The general mechanism works as follows: firstly the liquid crystal favors a particular alignment on the dopants surface due to surface treatment. Secondly the dopants themselves interact with externally applied fields favoring a particular alignment. These two mechanisms in conjunction transfer the electromagnetic torque applied to the dopants to the nematic through the surface anchoring. This allows the

*KRD was funded by BB/J000868/1 and by ERC consolidation grant 646809 during the completion of this work.

†Mathematical Sciences, University of Southampton, Southampton, England, UK

‡Engineering Sciences, University of Southampton, Southampton, England, UK

geometry and physical make up of the dopants to modulate the strength of the interaction. In addition, dopants exclude volume from the system reducing the strength of the elastic interaction within the nematic.

Mean field theories, such as those that describe ferromagnetic [10, 11] or ferroelectric [26, 42] colloidal suspensions, introduce an effective free energy. For example, the free energy proposed by Burylov and Raikher contains additional terms to describe (*i*) the interaction of the dopant with the applied magnetic field, (*ii*) a mixing entropy which allows for concentration gradients and (*iii*) the surface interaction between the nematic and dopant. However, the macroscopic parameters that control these interactions are not defined within the theory and must be determined separately.

In this paper we use homogenization to derive an effective model of a nematic liquid crystal doped with perfectly conducting particles in the weak anchoring case, i.e. in the absence of defects. As mentioned previously, this case is of most interest for light-based applications, as the colloidal suspension is optically homogeneous. The model can be seen as an extension of that developed in [6] to incorporate rotating particles. In [6] the case of static inclusions that may be identified with dopant particles or a micro-structure is studied. In this paper we study a two-dimensional system of liquid crystal and dopant particles in which the dopant particles may freely rotate. Homogenization theory [33] is a set of tools for extracting the limiting behavior of a system in the limit of vanishing micro-structure. It is particularly suited for approximately periodic systems in which the period of the micro-structure is small in comparison to some characteristic macroscopic length. We treat the colloid as a system of periodic cells each containing one colloidal particle; the orientation of the particles is allowed to change between cells, i.e. the system is only locally periodic. There is a large literature on locally-periodic homogenization [1, 7, 8, 14, 27, 29, 35, 43]. Here we follow in particular the approach by Richardson *et al.* [38] and Bruna and Chapman [9]. We obtain a set of stiff macroscopic equations using homogenization. To simplify the numerical verification we extract the slow time-scale dynamics that corresponds to the elastic reorientation of the nematic from our macroscopic model using the method outlined in [15].

The final macroscopic equations we arrive at are given in section 3.5: they approximate the behavior of the applied field, the particles and the nematic. These equations show that the mixture possesses different material parameters than the pure nematic, namely reduced elasticity and enhanced electrical susceptibility. In addition, the dopant particles are aligned by torques due to the nematic and electric field. As we do not allow the particles to move from a periodic lattice, we do not obtain a mixing entropy contribution. We also find no change to the scalar order parameter.

Our model differs from those of Burylov [10], [11] and Shelestiuk [42] and Lopatina and Selinger [26] in two ways: first, we consider a different system, metallic particles with an externally applied electric field. This choice, however, is only a matter of algebraic and modeling convenience and we could relatively easily include other classes of particles. The bigger difference is that our model is based on a formal up-scaling approach from which we obtain a sequence of cell problems that capture the effects of different particle shapes in a single general picture. The result is that the macroscopic parameters are defined uniquely in terms of the microscopic properties of the dopant.

The structure of the paper is as follows: in section 2 we derive the microscopic equations governing the nematic, particles, flow and applied field; in section 3 we derive the homogenized equations which approximate the macroscopic behavior of our system; in section 4 we validate our model against finite element simulations of a

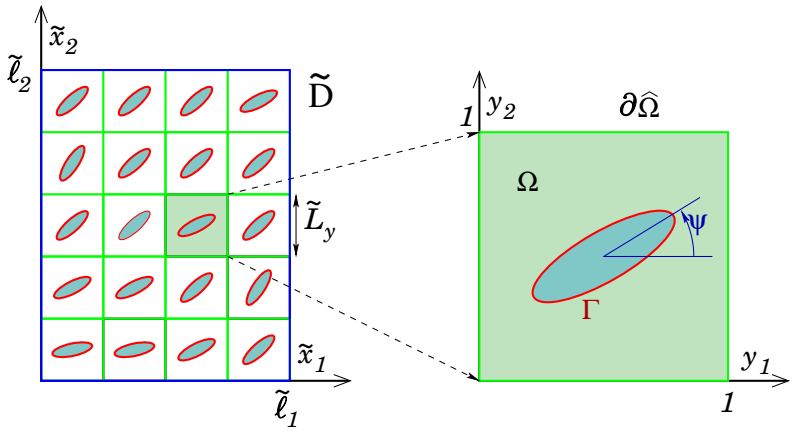


FIG. 2.1. *Schematic of a planar domain containing a liquid crystal doped with nanoparticles. The left hand side represents the domain of the microscopic model,* $\tilde{\mathrm{D}}$ *(rectangle minus the particles). This microscopic domain is formed by a tessellation of perforated squares of size* $\tilde{L}_y$ *each with one hole, corresponding to a particle; it is parameterized by (dimensional) coordinates* $\tilde{x}_j$*, with* $0 \le \tilde{x}_j \le \tilde{\ell}_j$*,* $j = 1, 2$*. The right hand side is a generic cell domain* $\Omega$ *parameterized by (non-dimensional) coordinates* $\boldsymbol{y}$*, with* $0 \le y_j \le 1$*,* $j = 1, 2$*. Each cell domain has outer boundary* $\partial\hat{\Omega}$ *and contains a particle with boundary* $\Gamma$ *and orientation parameterized by an angle* $\psi$*.*

large but computationally feasible number of particles in a nematic liquid crystal. We discuss the model and possible future work in section 5 and finally present conclusions in section 6.

**2. Microscopic model.** In this section we derive the microscopic equations governing the liquid crystal suspension that we are going to study in the following sections.

**2.1. Representing the system.** Metallic dopant particles added to a nematic liquid crystal act to alter the elastic and dielectric properties of the nematic. To determine the governing equations for the nematic and dopant particles we use a free energy and dissipation principle (Rayleigh principle). We assume that the particles are sufficiently dispersed that we may approximate them as lying on a lattice. We consider a nematic liquid crystal in a two-dimensional planar geometry, confined to a microscopic domain $\tilde{\mathrm{D}}$ given by the difference between the rectangle $[0, \tilde{\ell}_1] \times [0, \tilde{\ell}_2]$ and all the particles[1]. The microscopic domain is parameterized by dimensional coordinates $\tilde{x}_j$, $j = 1, 2$ and depends on the size and orientation of the particles. The perfectly conductive particles have rotation but not translation freedom and are arrayed on a lattice (see left-hand side of figure 2.1). An electrostatic potential of given amplitude is applied to the liquid crystal to change its orientation. We assume that the alignment of the liquid crystal and the value of the electrostatic potential are assigned on the outer boundary of the rectangle (blue line in figure 2.1). In particular,

[1]Three domains are used in this paper: the *microscopic* domain $\tilde{\mathrm{D}}$ is the domain of definition of the microscopic model described in this section and is parameterized by the coordinates $\tilde{\boldsymbol{x}}$. There is also a non-dimensional version of this domain; it is indicated with the symbol D and is parameterized by the coordinates $\boldsymbol{x}$. The *cell* domain $\Omega$ corresponds to the square around a single particle and is parameterized by the microscopic coordinates $\boldsymbol{y}$ (see section 3). The *macroscopic* domain $\mathrm{D}_H$ is the domain of definition of the homogenized equation (see table 2.1 and section 3.4.3) and is parameterized by the coordinates $\boldsymbol{x}$.

in the numerical simulations we will assume that the system is periodic in the $\tilde{x}_1$ direction with period $\tilde{\ell}_1$ and the electrostatic potential and alignment of the liquid crystal are fixed on the top and bottom boundary. The restrictions to two dimensions is made for algebraic and computational simplicity. We discuss in the conclusions the work involved in extending the equations presented here to three dimensions. The total free energy of the system is

$$\tilde{F}_{\text{tot}} = \int_{\tilde{\mathrm{D}}} \left( \tilde{\mathcal{F}}_B + \tilde{\mathcal{F}}_E \right) d\tilde{S} + \int_{\mathcal{B}_{\tilde{\mathrm{D}}}} \tilde{\mathcal{F}}_S d\tilde{l}, \tag{2.1}$$

with $\tilde{\mathcal{F}}_S$, $\tilde{\mathcal{F}}_E$ $\tilde{\mathcal{F}}_B$ the surface, electrostatic and bulk free energy densities respectively. The surface free energy is evaluated on the boundary $\mathcal{B}_{\tilde{\mathrm{D}}}$ between the microscopic domain $\tilde{\mathrm{D}}$ and all the particles (red curves in figure 2.1). We represent the orientation of the nematic using the $\mathcal{Q}$-tensor [16]. Very roughly, a uniaxial liquid crystal is formed by cylindrically symmetric elongated molecules that have a non-zero average orientation, called the *director*. It is intuitive to represent the director using a unit vector $\hat{\boldsymbol{d}}$. However, this representation is mathematically inaccurate: the molecules and, hence, the director have inversion symmetry, i.e. $\hat{\boldsymbol{d}}$ and $-\hat{\boldsymbol{d}}$ correspond to the same liquid crystalline state. We are therefore required to represent the director using a tensor $\mathcal{Q}$ that is quadratic in $\hat{\boldsymbol{d}}$: the director is the eigenvector with largest eigenvalue. In general the $\mathcal{Q}$-tensor is a $3 \times 3$ traceless symmetric matrix. However, in this paper we assume that the director is oriented within the $(\tilde{x}_1, \tilde{x}_2)$-plane. Hence we can describe the nematic liquid crystal using a two dimensional $\mathcal{Q}$-tensor theory. For a nematic locally aligned with a director $\hat{\boldsymbol{d}}$, the $\tilde{\mathcal{Q}}$-tensor is given by

$$\tilde{\mathcal{Q}} = \sqrt{2}\tilde{S}\left( \hat{\boldsymbol{d}} \otimes \hat{\boldsymbol{d}} - \frac{1}{2}\mathcal{I} \right), \tag{2.2}$$

where $\tilde{S}$ the scalar order parameter and $\mathcal{I}$ is the $2 \times 2$ identity matrix. The scalar order parameter is a function of temperature that measures the degree of ordering: it is zero in the isotropic phase and unity in the fully nematic phase. The normalization in equation (2.2) is chosen so that $\mathrm{Tr}(\tilde{\mathcal{Q}}^2) = \tilde{S}^2$. Traceless symmetric $2 \times 2$ tensors forms a two-dimensional vector space. Following Gartland *et al.* [19], we expand the $\mathcal{Q}$-tensor as $\tilde{\mathcal{Q}} = \sum_{i=1}^{2} \tilde{a}_i \mathcal{T}^{(i)}$ where

$$\mathcal{T}^{(1)} = \frac{1}{\sqrt{2}} \begin{bmatrix} -1 & 0 \\ 0 & 1 \end{bmatrix}, \quad \mathcal{T}^{(2)} = \frac{1}{\sqrt{2}} \begin{bmatrix} 0 & 1 \\ 1 & 0 \end{bmatrix}, \tag{2.3}$$

form a basis of the tensor space and $\tilde{a}_i = \mathrm{Tr}(\tilde{\mathcal{Q}}\mathcal{T}^{(i)})$ are the components of $\tilde{\mathcal{Q}}$ on this basis. The dimensional bulk free energy density in the single elastic constant approximation is

$$\tilde{\mathcal{F}}_B = \frac{\tilde{L}}{2} \|\tilde{\boldsymbol{\nabla}} \tilde{\boldsymbol{a}}\|^2 + \frac{1}{2} A \left( T - T^* \right) |\tilde{\boldsymbol{a}}|^2 + \frac{1}{4} C |\tilde{\boldsymbol{a}}|^4, \tag{2.4}$$

where $\tilde{L}$ is the elastic constant, $\tilde{\boldsymbol{a}} = [\tilde{a}_1 \ \tilde{a}_2]^T$ is a vector formed from the components of the $\tilde{\mathcal{Q}}$ tensor on the basis of traceless symmetric tensors $\mathcal{T}^{(i)}, i = 1, 2$, $A$ and $C$ are thermotropic coefficients, $T$ is the absolute temperature with $T^*$ the critical temperature at which the isotropic phase becomes unstable. The dielectric energy density written in terms of the electric field $\tilde{\boldsymbol{E}}$ and relative dielectric tensor $\epsilon$ is given by

$$\tilde{\mathcal{F}}_E = -\frac{1}{2} \tilde{\boldsymbol{E}} \cdot (\epsilon_0 \epsilon \tilde{\boldsymbol{E}}) \tag{2.5}$$

with

$$\epsilon = \epsilon_u \mathcal{I} + \frac{\Delta\epsilon}{\sqrt{2}}\tilde{\mathcal{Q}}. \tag{2.6}$$

Here $\epsilon_0$ is the permittivity of free space, $\epsilon_u \equiv (\epsilon_\parallel + \epsilon_\perp)/2$ and $\Delta\epsilon \equiv \epsilon_\parallel - \epsilon_\perp$ are the uniform and anisotropic part of the dielectric permittivity in the fully nematic phase ($\tilde{S} = 1$), with $\epsilon_\parallel$ and $\epsilon_\perp$ the corresponding extraordinary and ordinary dielectric permittivity, respectively. The surface energy density is given by

$$\tilde{\mathcal{F}}_S = \frac{\tilde{\mu}}{2}|\tilde{\boldsymbol{a}} - \tilde{\boldsymbol{a}}_S|^2, \tag{2.7}$$

where $\tilde{\mu}$ is the anchoring energy surface density and $\tilde{\boldsymbol{a}}_S$ the preferred alignment on the particle surface. The dynamics are given by the dissipation function $\tilde{R}$ [44], the energy lost per unit volume and unit time due to viscous dissipation,

$$\tilde{R} = \frac{1}{2}\zeta_1 \left|\mathring{\tilde{\boldsymbol{a}}}\right|^2 + \frac{\zeta_3}{2}\tilde{\mathcal{D}} : \tilde{\mathcal{D}}. \tag{2.8}$$

Here

$$\mathring{\tilde{\boldsymbol{a}}} = \frac{\partial \tilde{\boldsymbol{a}}}{\partial \tilde{t}} + \tilde{\boldsymbol{v}} \cdot \tilde{\boldsymbol{\nabla}}\tilde{\boldsymbol{a}} - 2\tilde{W}\tilde{\boldsymbol{a}} \tag{2.9}$$

is the corotational derivative[2] of $\tilde{\mathcal{Q}}$ expressed in terms of the component vector $\tilde{\boldsymbol{a}}$, $\boldsymbol{v}$ is the fluid velocity,

$$\tilde{W}_{ij} = \frac{1}{2}\left(\tilde{v}_{i,j} - \tilde{v}_{j,i}\right) \tag{2.10}$$

is the vorticity,

$$\tilde{\mathcal{D}}_{ij} = \frac{1}{2}\left(\tilde{v}_{i,j} + \tilde{v}_{j,i}\right) \tag{2.11}$$

is the symmetric part of the velocity gradient, $\tilde{v}_{i,j} = \frac{\partial \tilde{v}_i}{\partial \tilde{x}_j}$, $\zeta_3$ (up to a factor of 1/2) is the isotropic part of the nematic viscosities and $\zeta_1 \equiv \frac{\gamma_1}{2\tilde{S}^2}$ with $\gamma_1$ is the rotational viscosity. We use a simplified version of the dissipation function proposed by Sonnet *et al.* [44] and include only two terms in the dissipation: the rotational viscosity of the nematic, which sets the time scale of $\tilde{\mathcal{Q}}$, and the isotropic viscosity, which sets the time scale of the particles. In general the details of the dynamic response of a liquid crystal system depend on a (system dependent) combination of viscosity coefficients. However, out of all of these viscosities, the rotational viscosity always plays a large role in setting the time-scale on which the liquid crystal reorients. Similarly, the drag on the colloidal particles will in general depend on a complicated combination of viscosity coefficients determined by the local orientation of the nematic, velocity and velocity gradient. However, the isotropic viscosity always plays a large role in determining the viscous stress on the particles. Including these two terms in the dissipation therefore represents the simplest model which posses the correct symmetries and likely captures the main aspects of the dynamic response of the system. In general we expect that this approximation will be valid for slowly evolving systems.

[2]The corotational derivative describes how the director changes in a frame that rotates with the fluid element [44, 45]

In addition to neglecting the coupling of the flow to the $\mathcal{Q}$-tensor, we also neglect the inertia of the fluid. This is a standard assumption when analyzing liquid crystal devices. In our system we can justify this approximation because requiring that the Reynolds number is small,

$$\mathrm{Re} = \frac{2\rho|\tilde{\boldsymbol{v}}|\tilde{\ell}_2}{\zeta_3} \ll 1. \tag{2.12}$$

with $\rho$ the density of the nematic and $\tilde{\ell}_2$ the characteristic size of the system, gives $|\tilde{\boldsymbol{v}}| \lesssim 10^2$ ms$^{-1}$, a condition that is easily satisfied in most liquid crystal devices.

Finally, to obtain the torque on the dopants caused by fluid flow and the electric field we use the viscous and Maxwell stress tensors. The first is [44],

$$\tilde{T}^{(N)} = -\tilde{p}\mathcal{I} - \tilde{L}\tilde{\boldsymbol{\nabla}}\tilde{\boldsymbol{a}}\cdot\tilde{\boldsymbol{\nabla}}\tilde{\boldsymbol{a}} + \zeta_1\left[(\mathcal{W}\tilde{\boldsymbol{a}})\cdot\left(\frac{\partial\tilde{\boldsymbol{a}}}{\partial\tilde{t}} + \tilde{\boldsymbol{v}}\cdot\tilde{\boldsymbol{\nabla}}\tilde{\boldsymbol{a}}\right)\mathcal{W} + 2\tilde{W}|\tilde{\boldsymbol{a}}|^2\right] + \zeta_3\tilde{\mathcal{D}}, \tag{2.13}$$

where $\tilde{p}$ is the pressure and

$$\mathcal{W} = \begin{bmatrix} 0 & -1 \\ 1 & 0 \end{bmatrix}. \tag{2.14}$$

The Maxwell stress tensor is

$$\tilde{T}^{(M)} = \tilde{\boldsymbol{E}}\otimes\tilde{\boldsymbol{D}} - \frac{1}{2}\left(\tilde{\boldsymbol{E}}\cdot\tilde{\boldsymbol{D}}\right)\mathcal{I}, \tag{2.15}$$

where $\tilde{\boldsymbol{D}} = \epsilon_0\epsilon\tilde{\boldsymbol{E}}$ is the electric displacement field.

**2.2. Nondimensionalization.** Before we derive the microscopic model from the free energies and dissipation function defined in the previous section, we must first nondimensionalize equations (2.4), (2.5), (2.7) and (2.8). All the scaling coefficients and scaled parameters are listed in table 2.1. Some typical values are listed in table 2.2. Note that $\xi_0^2$ and, hence, $\chi_a$ are very small. We will make use of this property in sections 3.3 and 3.5 to simplify the macroscopic equations. The bulk and surface nondimensional free energy densities and the total free energy are given by

$$\mathcal{F}_B = \frac{\xi_0^2}{2}\|\boldsymbol{\nabla}\boldsymbol{a}\|^2 - \frac{1}{2}|\boldsymbol{a}|^2 + \frac{1}{4}|\boldsymbol{a}|^4, \tag{2.16a}$$

$$\mathcal{F}_E = -\chi_u|\boldsymbol{E}|^2 - \chi_a\boldsymbol{a}\cdot\boldsymbol{e}, \tag{2.16b}$$

$$\mathcal{F}_S = \frac{\beta}{2}|\boldsymbol{a}_S - \boldsymbol{a}|^2, \tag{2.16c}$$

$$F_{\mathrm{tot}} = \int_{\mathrm{D}}\mathcal{F}_{\mathrm{tot}}\,dS + \int_{\mathcal{B}_{\mathrm{D}}}\mathcal{F}_S\,dl, \tag{2.16d}$$

where D is the nondimensional microscopic domain, given by the difference between the rectangle $\mathrm{D}_H = [0,\ell]\times[0,1]$ and all the particles, $\mathcal{B}_{\mathrm{D}}$ is its boundary with all the particles and the total bulk free energy density is

$$\mathcal{F}_{\mathrm{tot}} = \mathcal{F}_B + \mathcal{F}_E\,. \tag{2.17}$$

We have defined a traceless electric tensor by analogy to (2.2),

$$\mathcal{E} = \sqrt{2}\left(\boldsymbol{E}\otimes\boldsymbol{E} - \frac{1}{2}\mathcal{I}|\boldsymbol{E}|^2\right), \tag{2.18}$$

| | |
|---|---|
| Order parameter scaling factor | $S_0 = [A(T^* - T)/C]^{1/2}$ |
| Director tensor and components | $(\tilde{\mathcal{Q}}, \tilde{\boldsymbol{a}}) = S_0(\mathcal{Q}, \boldsymbol{a})$ |
| Total bulk free energy density | $\tilde{\mathcal{F}}_{\rm tot} = CS_0^4 \mathcal{F}_{\rm tot}$ |
| Macroscopic spatial coordinates | $\tilde{\boldsymbol{x}} = \tilde{\ell}_2 \boldsymbol{x}$ |
| Aspect ratio of the microscopic domain | $\ell = \tilde{\ell}_1/\tilde{\ell}_2$ |
| Nondimensional macroscopic domain | $\mathrm{D}_H = [0, \ell] \times [0, 1]$ |
| Voltage scaling factor | $\tilde{V}_0 = [4\tilde{L}S_0/\epsilon_0]^{1/2}$ |
| Electric field | $\tilde{\boldsymbol{E}} = (\tilde{V}_0/\tilde{\ell}_2)\boldsymbol{E}$ |
| Elastic constant | $\xi_0^2 = \tilde{L}/(\tilde{\ell}_2^2 C S_0^2)$ |
| Isotropic dielectric permittivity | $\chi_u = 2\epsilon_u \xi_0^2/S_0$ |
| Electric coupling coefficient | $\chi_a = \Delta\epsilon \xi_0^2$ |
| Anchoring strength | $\beta = \tilde{\mu}\tilde{\ell}_2 \xi_0^2/\tilde{L}$ |
| Reduced viscosity | $\zeta' = \zeta_3/(\zeta_1 S_0^2)$ |
| Time scaling factor | $\tau = \zeta_1/(CS_0^2)$ |
| Dissipation function | $\tilde{R} = RCS_0^4/\tau$ |
| Time | $\tilde{t} = \tau t$ |
| Pressure | $\tilde{p} = CS_0^2 p$ |
| Velocity | $\tilde{\boldsymbol{v}} = (\tilde{\ell}_2/\tau)\boldsymbol{v}$ |
| Velocity gradient & vorticity | $(\tilde{\mathcal{D}}, \tilde{W}) = (\mathcal{D}, W)/\tau$ |
| Anchoring to elastic energy ratio | $W_A = \tilde{\mu}\tilde{\ell}_2/\tilde{L}$ |
| Reduced dielectric tensor | $\hat{\epsilon} = \epsilon/\epsilon_u$ |
| Dielectric anisotropy coefficient | $\alpha = \Delta\epsilon S_0/(\sqrt{2}\epsilon_u)$ |

TABLE 2.1

*Scaled variables and parameters, and scaling coefficients needed for the nondimensionalization of the colloidal nematic equations (see section 2.2). The unscaled variables are identified by a superscript ˜.*

| | | |
|---|---|---|
| $T - T^* = -10\ K$ | $A = 0.13 \cdot 10^6\ \mathrm{JK^{-1}m^{-3}}$ | $C = 3.9 \cdot 10^6\ \mathrm{JK^{-1}m^{-3}}$ |
| $\tilde{L} = 10^{-11}\ \mathrm{N}$ | $\zeta_1 = 280\ \mathrm{mPa\ s}$ | $\zeta_3 = 220\ \mathrm{mPa\ s}$ |
| $\tilde{\ell}_2 = 32 \cdot 10^{-6}\ \mathrm{m}$ | $\epsilon_{\parallel} = 20$ | $\epsilon_{\perp} = 5$ |
| $S_0 \approx 0.6$ | $\xi_0^2 \approx 10^{-8}$ | $[\chi_u, \chi_a] \approx [10^{-6}, 10^{-7}]$ |
| $\tilde{\mu} = 10^{-7}\,\mathrm{to}\,10^{-5}\mathrm{Jm^{-2}}$ | $W_A \approx 0.1\,\mathrm{to}\,10$ | $\beta \approx 3 \cdot 10^{-9}\,\mathrm{to}\,3 \cdot 10^{-7}$ |

TABLE 2.2

*Typical parameter values (based on those for 5CB reported in[4]). These are used in section 3.5 to justify the multiscale analysis and in the numerical simulations in section 4.*

such that $\mathrm{Tr}(\mathcal{E}^2) = |\boldsymbol{E}|^2$. The vector $\boldsymbol{e}$ that appears equation (2.16b) is formed by its components on the basis (2.3).

The nondimensional dissipation function is given by

$$R = \frac{1}{2}|\mathring{\boldsymbol{a}}|^2 + \frac{1}{2}\zeta'\mathcal{D} : \mathcal{D}, \tag{2.19}$$

where all the scaled variables are defined in table 2.1. The corotational derivative $\mathring{\boldsymbol{a}}$ is defined by equation (2.9) with the dimensional variables replaced by the corresponding nondimensional versions:

$$\mathring{\boldsymbol{a}} = \frac{\partial \boldsymbol{a}}{\partial t} + \boldsymbol{v}\cdot\boldsymbol{\nabla}\boldsymbol{a} - 2W\boldsymbol{a}. \tag{2.20}$$

The Maxwell (2.15) and viscous (2.13) stress tensors become

$$T^{(M)} = \chi_u\left[\boldsymbol{E}\otimes\boldsymbol{D} - \frac{1}{2}(\boldsymbol{E}\cdot\boldsymbol{D})\mathcal{I}\right], \tag{2.21a}$$

$$T^{(N)} = -p\mathcal{I} - \xi_0^2\boldsymbol{\nabla}\boldsymbol{a}\cdot\boldsymbol{\nabla}\boldsymbol{a} + (\mathcal{W}\boldsymbol{a})\cdot\left(\frac{\partial \boldsymbol{a}}{\partial t} + \boldsymbol{v}\cdot\boldsymbol{\nabla}\boldsymbol{a}\right)\mathcal{W} + 2W|\boldsymbol{a}|^2 + \zeta'\mathcal{D}. \tag{2.21b}$$

The nondimensional electric displacement field $\boldsymbol{D}$ is related to the nondimensional electric field by

$$\boldsymbol{D} = \hat{\epsilon}\boldsymbol{E}, \tag{2.22}$$

with $\hat{\epsilon}$ the reduced dielectric permittivity tensor, $\epsilon = \epsilon_u\hat{\epsilon}$.

Having expressed all the free energies and stress tensors in nondimensional form, we are now in position to derive the equations governing the nematic liquid crystal, fluid flow, dopants and applied potential.

**2.3. The nematic equations.** The equations governing the nematic liquid crystal dynamics are given by,

$$\frac{\partial R}{\partial \mathring{\boldsymbol{a}}} = \boldsymbol{\nabla}\cdot\frac{\partial \mathcal{F}_{\mathrm{tot}}}{\partial \boldsymbol{\nabla}\boldsymbol{a}} - \frac{\partial \mathcal{F}_{\mathrm{tot}}}{\partial \boldsymbol{a}} \tag{2.23}$$

in the bulk and

$$\hat{\boldsymbol{n}}\cdot\frac{\partial \mathcal{F}_{\mathrm{tot}}}{\partial \boldsymbol{\nabla}\boldsymbol{a}} = -\frac{\partial \mathcal{F}_S}{\partial \boldsymbol{a}} \tag{2.24}$$

on $\mathcal{B}_{\mathrm{D}}$, with $\hat{\boldsymbol{n}}$ the outward unit normal from D.

Substituting the total nondimensional free energy density from (2.16) and the dissipation function from equation (2.19) into (2.23) and (2.24) we find the nematic is governed by

$$\mathring{\boldsymbol{a}} = \xi_0^2\nabla^2\boldsymbol{a} + \chi_a\boldsymbol{e} + \boldsymbol{a} - \boldsymbol{a}|\boldsymbol{a}|^2, \qquad \boldsymbol{x}\in\mathrm{D}, \tag{2.25a}$$

$$\hat{\boldsymbol{n}}\cdot\boldsymbol{\nabla}\boldsymbol{a} = W_A\left(\boldsymbol{a}_S - \boldsymbol{a}\right), \qquad \boldsymbol{x}\in\mathcal{B}_{\mathrm{D}}, \tag{2.25b}$$

$$\boldsymbol{a} = \boldsymbol{b}(\boldsymbol{x}), \qquad \boldsymbol{x}\in\mathcal{O}_{\mathrm{D}}, \tag{2.25c}$$

where $W_A \equiv \frac{\beta}{\xi_0^2} = \frac{\tilde{\mu}\tilde{\ell}_2}{\tilde{L}}$ and $\boldsymbol{b}(\boldsymbol{x})$ is the prescribed alignment on $\mathcal{O}_{\mathrm{D}}$, the outer boundary of D.

**2.4. The particle equations.** To determine the governing equations for the particles we balance the torques due to the fluid flow, nematic liquid crystal and electric fields. These torques can each be determined using the appropriate stress tensor or the free energy and dissipation function. We use the latter to derive the nematic torques and the former to determine the electrostatic contribution.

The torque on a particle due to elastic distortions and surface orientations is equal to minus the derivative of the nematic elastic and surface free energy density with respect to particle orientation,

$$\begin{aligned}\tilde{\tau}_N = &-\int_{\Gamma_{\boldsymbol{x}}} \left(\frac{\xi_0^2}{2}\|\boldsymbol{\nabla a}\|^2 - \frac{1}{2}|\boldsymbol{a}|^2 + \frac{1}{4}|\boldsymbol{a}|^4\right)\left(\hat{\boldsymbol{n}}\cdot\frac{\partial \boldsymbol{r}_{\boldsymbol{x}}}{\partial\psi}\right) dl_{\boldsymbol{x}} \\ &-\int_{\Gamma_{\boldsymbol{x}}} \left[\beta\left(\boldsymbol{a}_S - \boldsymbol{a}\right)\cdot\frac{\partial \boldsymbol{a}_S}{\partial\psi} + \frac{\beta^2}{\xi_0^2}\left(\hat{\boldsymbol{n}}\cdot\frac{\partial \boldsymbol{r}_{\boldsymbol{x}}}{\partial\psi}\right)|\boldsymbol{a}_S - \boldsymbol{a}|^2\right. \\ &\left.+\frac{\beta\kappa_{\boldsymbol{x}}}{2}\left(\hat{\boldsymbol{n}}\cdot\frac{\partial \boldsymbol{r}_{\boldsymbol{x}}}{\partial\psi}\right)|\boldsymbol{a}_S - \boldsymbol{a}|^2\right] dl_{\boldsymbol{x}},\end{aligned} \tag{2.26}$$

where $dl_{\boldsymbol{x}}$ is the line element in the $\boldsymbol{x}$ coordinates, $\psi$ is the particle alignment angle, $\Gamma_{\boldsymbol{x}}$ is the boundary of an *individual* particle parameterized using the $\boldsymbol{x}$-coordinates and we have used Reynolds transport theorem (see section SM1 of the Supplementary material). Here $\boldsymbol{r}_{\boldsymbol{x}}$ is the position vector on the particle boundary with respect to a given origin in the $\boldsymbol{x}$ coordinate system and $\kappa_{\boldsymbol{x}}$ is its curvature,

$$\kappa_{\boldsymbol{x}} = \left|\frac{\partial \boldsymbol{r}_{\boldsymbol{x}}}{\partial\psi}\times\frac{\partial^2 \boldsymbol{r}_{\boldsymbol{x}}}{\partial\psi^2}\right|\cdot\left|\frac{\partial \boldsymbol{r}_{\boldsymbol{x}}}{\partial\psi}\right|^{-3} \tag{2.27}$$

To compute the torque due to the electric field we use the Maxwell stress tensor (2.21a). The $x_3$ component of the torque is

$$\tau_E = -\int_{\Gamma_{\boldsymbol{x}}} r_{\boldsymbol{x}\perp k}\hat{n}_m T^{(M)}_{km}\, dl_{\boldsymbol{x}}, \tag{2.28}$$

where we sum over repeated indices with the indices ranging from 1 to 2. Here $\boldsymbol{r}_{\boldsymbol{x}\perp} = [-x_2, x_1]^T$.

The torque or drag due to fluid flow sets the time-scale of the particle motion. In nondimensional units the flow velocity $\boldsymbol{v}$ is governed by the divergence of the stress tensor [44]

$$\frac{\zeta'}{2}\nabla^2\boldsymbol{v} = \boldsymbol{\nabla}p + \xi_0^2\boldsymbol{\nabla}\cdot(\boldsymbol{\nabla a}\cdot\boldsymbol{\nabla a}) - \mathcal{W}\boldsymbol{\nabla}(\boldsymbol{a}\mathcal{W}\mathring{\boldsymbol{a}}), \qquad \boldsymbol{x}\in \mathrm{D}, \tag{2.29a}$$

$$\boldsymbol{\nabla}\cdot\boldsymbol{v} = 0, \qquad \boldsymbol{x}\in \mathrm{D}, \tag{2.29b}$$

$$\boldsymbol{v} = \frac{\partial\psi}{\partial t}\boldsymbol{r}_{\boldsymbol{x}\perp}, \qquad \boldsymbol{x}\in \mathcal{B}_{\mathrm{D}}, \tag{2.29c}$$

$$\boldsymbol{v} = 0, \qquad \boldsymbol{x}\in \mathcal{O}_{\mathrm{D}}. \tag{2.29d}$$

We can now compute the drag on the particle from the dynamic stress tensor. Fol-

lowing the same method as for the Maxwell stress we find two contributions,

$$
\begin{aligned}
(\tau_v)_3 &= -\int_{\Gamma_{\boldsymbol{x}}} r_{\boldsymbol{x}\perp k}\hat{n}_m T^{(N)}_{mk}\, dl_{\boldsymbol{x}} \\
&= -\int_{\Gamma_{\boldsymbol{x}}} \boldsymbol{r}_{\boldsymbol{x}\perp}\cdot(-p\hat{\boldsymbol{n}}+\zeta'\mathcal{D}\hat{\boldsymbol{n}}) \\
&\quad -\int_{\Gamma_{\boldsymbol{x}}} \left\{\boldsymbol{r}_{\boldsymbol{x}\perp}\cdot\hat{\boldsymbol{n}}\left[(\mathcal{W}\boldsymbol{a})\cdot\left(\frac{\partial \boldsymbol{a}}{\partial t}+\boldsymbol{v}\cdot\boldsymbol{\nabla}\boldsymbol{a}\right)\right]+2|\boldsymbol{a}|^2\boldsymbol{r}_{\boldsymbol{x}\perp}\cdot(W\hat{\boldsymbol{n}})\right\} dl_{\boldsymbol{x}}. \qquad (2.30)
\end{aligned}
$$

Summarizing, the particle dynamics are governed by

$$
\begin{aligned}
&\int_{\Gamma_{\boldsymbol{x}}} \boldsymbol{r}_{\boldsymbol{x}\perp}\cdot(-p\hat{\boldsymbol{n}}+\zeta'\mathcal{D}\hat{\boldsymbol{n}})\, dl_{\boldsymbol{x}} \\
&\qquad +\int_{\Gamma_{\boldsymbol{x}}} \left\{\boldsymbol{r}_{\boldsymbol{x}\perp}\cdot\hat{\boldsymbol{n}}\left[(\mathcal{W}\boldsymbol{a})\cdot\left(\frac{\partial \boldsymbol{a}}{\partial t}+\boldsymbol{v}\cdot\boldsymbol{\nabla}\boldsymbol{a}\right)\right]+2|\boldsymbol{a}|^2\boldsymbol{r}_{\boldsymbol{x}\perp}\cdot(W\hat{\boldsymbol{n}})\right\} dl_{\boldsymbol{x}} = \\
&\qquad -\int_{\Gamma_{\boldsymbol{x}}} \left(\frac{\xi_0^2}{2}\|\boldsymbol{\nabla}\boldsymbol{a}\|^2-\frac{1}{2}|\boldsymbol{a}|^2+\frac{1}{4}|\boldsymbol{a}|^4\right)\left(\hat{\boldsymbol{n}}\cdot\frac{\partial \boldsymbol{r}_{\boldsymbol{x}}}{\partial\psi}\right) dl_{\boldsymbol{x}} \\
&\qquad -\int_{\Gamma_{\boldsymbol{x}}} \left[\beta\,(\boldsymbol{a}_S-\boldsymbol{a})\cdot\frac{\partial \boldsymbol{a}_S}{\partial\psi}+\frac{\beta^2}{\xi_0^2}\left(\hat{\boldsymbol{n}}\cdot\frac{\partial \boldsymbol{r}_{\boldsymbol{x}}}{\partial\psi}\right)|\boldsymbol{a}_S-\boldsymbol{a}|^2\right. \\
&\qquad\qquad \left.+\frac{\beta\kappa_{\boldsymbol{x}}}{2}\left(\hat{\boldsymbol{n}}\cdot\frac{\partial \boldsymbol{r}_{\boldsymbol{x}}}{\partial\psi}\right)|\boldsymbol{a}_S-\boldsymbol{a}|^2\right] dl_{\boldsymbol{x}} \\
&\qquad -\int_{\Gamma_{\boldsymbol{x}}} r_{\perp k}\hat{n}_l T^{(M)}_{lk}\, dl_{\boldsymbol{x}}. \qquad (2.31)
\end{aligned}
$$

**2.5. The potential equations.** The electric potential is governed by Maxwell's equation for the electric displacement field. We assume that there are no free charges in the system and impose a floating potential condition on the surface of the inclusions. In nondimensional form the equations governing the electric potential $\phi$ are

$$
\begin{aligned}
&\boldsymbol{\nabla}\cdot[(\mathcal{I}+\alpha\mathcal{Q})\,\boldsymbol{\nabla}\phi]=0, && \boldsymbol{x}\in \mathrm{D}, && \text{(2.32a)}\\
&\hat{\boldsymbol{t}}\cdot\boldsymbol{\nabla}\phi=0, && \boldsymbol{x}\in\mathcal{B}_{\mathrm{D}}, && \text{(2.32b)}\\
&\int_{\Gamma_{\boldsymbol{x}}}\hat{\boldsymbol{n}}\cdot[(\mathcal{I}+\alpha\mathcal{Q})\,\boldsymbol{\nabla}\phi]\, dl_{\boldsymbol{x}}=0, && && \text{(2.32c)}\\
&\phi(\boldsymbol{x})=\Phi(\boldsymbol{x}), && \boldsymbol{x}\in\mathcal{O}_{\mathrm{D}}, && \text{(2.32d)}
\end{aligned}
$$

where $\hat{\boldsymbol{t}}$ is the vector tangent to the particle, $\boldsymbol{E}=-\boldsymbol{\nabla}\phi$, $\alpha=\frac{\Delta\epsilon}{\epsilon_u}\frac{S_0}{\sqrt{2}}$ and $\Phi(\boldsymbol{x})$ is a prescribed potential on the outer surface of the microscopic domain. Equation (2.32a) is the first Maxwell equation for the (nondimensional) displacement field $\boldsymbol{D}$, defined in equation (2.22). Equation (2.32b) is the statement that the potential is constant on each particle (although it may vary from particle to particle). Equation (2.32c) requires that the total charge on each particle is zero. As the particles are metallic the local charge density is $\boldsymbol{D}\cdot\hat{\boldsymbol{n}}$; the integral of this quantity on the particle boundary $\Gamma_{\boldsymbol{x}}$ must be zero for the particle to be neutral.

**2.6. Summary of the microscopic model.** Equations (2.25), (2.29), (2.31) and (2.32) govern the nematic, fluid flow, particles and electric field in our system. We have assumed that the particles are fixed in position but are allowed to rotate freely,

thus neglecting any effect due to concentration gradients. The particles themselves are treated as ideal conductors and we use a continuum model for the nematic which bounds the minimum particle size that we may consider. Additionally by decoupling the nematic from the fluid flow we have included only limited, but realistic, dynamics. We perform a multiple scale analysis of these equations and by using a level set representation of the particles we derive homogenized equations. Following this we use a second method of multiple scales to extract the slow dynamics of the nematic.

## 3. Homogenization.

**3.1. Introduction.** As shown in figure 2.1 the microscopic domain D of the liquid crystal is formed by a tessellation of perforated squares of size $\tilde{L}_y$. To perform asymptotic homogenization we assume that $\tilde{L}_y \ll \tilde{\ell}_2$ and that the system is locally periodic, i.e. the director alignment, electrostatic potential and particle angle changes only a scale much longer than $\tilde{L}_y$. We consider each perforated square as a unit cell $\Omega$. We introduce a small parameter $\eta = \frac{\tilde{L}_y}{\tilde{\ell}_2}$, the ratio of the size of a unit cell (typical inter–particle spacing) $\tilde{L}_y$ to the size of the full system $\tilde{\ell}_2$. This small parameter allows us to define a second coordinate in our system $\boldsymbol{y} = \frac{\boldsymbol{x}}{\eta}$ which is defined within a unit cell only (see right hand side of figure 2.1). The unit cell has $\boldsymbol{y}$ coordinates $0 \leq y_j \leq 1$, with $j = 1, 2$. We call the generic unit cell the *cell* domain and we refer to it with the symbol $\Omega$. Its boundary is formed of two parts (see right hand side of figure 2.1): $\Gamma$ is the boundary with the particle in the $\boldsymbol{y}$ coordinate system (as opposed to $\Gamma_{\boldsymbol{x}}$, which represents the same curve, but parameterized by the $\boldsymbol{x}$-coordinates); $\partial\hat{\Omega}$ is the boundary shared with the neighboring unit cells. Finally, each unit cell $\Omega$ and, hence, particle angle $\psi$ and boundary $\Gamma$ can in principle be identified by the $\boldsymbol{x}$ coordinate of the cell center. In the homogenization limit $\eta \to 0$ the cell structure becomes a continuous and the particle angle becomes a field $\psi(\boldsymbol{x})$ that parametrizes the boundary $\Gamma$ and cell domain $\Omega$.

We seek governing equations in the limit as $\eta$ tends to zero. For a problem involving a generic field $u$ this is achieved by postulating that all fields are functions of both the macroscopic and microscopic coordinate, $u = u(\boldsymbol{x}, \boldsymbol{y})$. Next we make a series expansion in integer powers of the small parameter $\eta$, $u = u_0 + \eta u_1 + \eta^2 u_2 + O(\eta^3)$. We also use the chain rule to expand the gradient operator

$$\boldsymbol{\nabla} = \boldsymbol{\nabla}_{\boldsymbol{x}} + \frac{1}{\eta}\boldsymbol{\nabla}_{\boldsymbol{y}}, \tag{3.1}$$

capturing rapid variations on the small scale. By substituting the expansion of $u$ into the equations governing $u$ and expanding in powers of $\eta$ we obtain a sequence of equations for $u_0$, $u_1$ and $u_2$ in terms of the independent variables $\boldsymbol{x}$ and $\boldsymbol{y}$. Our aim is now to eliminate the $\boldsymbol{y}$-dependence from these equations leaving a set of macroscopic equations that depend only on the $\boldsymbol{x}$ variable. The key observations which allow us to proceed are that the geometry is locally periodic and that any variations on the $\boldsymbol{x}$ scale are small on the $\boldsymbol{y}$-scale and can, hence, be considered as a perturbation. At first order we generally obtain that $u_0$ varies only on the macro-scale. The parameters in the macroscopic equations are determined at next order by a series of cell problems which depend on the microscale geometry. Finally, by expanding to the following order and by enforcing solvability conditions, we obtain the macroscopic (homogenized) equations which governs $u_0(\boldsymbol{x})$.

Before applying the homogenization method outlined above to the microscopic model derived in section 2 we make two observations.

The first is that in our system we have two small parameters, $\eta$ and $\xi_0^2$ (see table 2.2) and we consider the limit that both of these parameters tend to zero. In the case of the liquid crystal, both of these limits are non–trivial: we will first deal with the case $\eta \to 0$ (section 3.4) and consider the second limit in section 3.5. In the case of the velocity equations the limit $\xi_0^2 \to 0$ is regular and trivial. The correct procedure is to first to derive a set of macroscopic equations for the velocity and then consider $\xi_0^2 \to 0$ in all equations. However, in the interest of readability and in order to reduce the number of terms carried forward at each term of the expansion, we take the limit $\xi_0^2 \to 0$ immediately (section 3.3), at the cost of a minor lack of formal rigor when mixing the expansion for the velocity and the alignment, as in equation (3.53).

The second observation concerns the scaling of the surface energy with $\eta$. As the size of the particles varies linearly with $\eta$, to avoid the surface term dominating the total free energy we postulate that the anchoring energy density scales linearly with $\eta$, i.e. $\tilde{\mu} = \mathcal{O}(\eta)$. As a consequence we write $\beta = \eta\beta_1$ and $W_A = \eta W_A^{(1)}$. A rough physical interpretation of this condition is that we have weak anchoring on the particle surface. More precisely in the limit $\eta \to 0$ the total boundary area between nematic and dopant diverges. As a result, unless we postulate a decrease in the anchoring energy density, we find that the surface anchoring dominates the particle dynamics. This limit is roughly physically equivalent to maintaining a constant volume of surfactant as the number of particles diverges. This way even though the total interaction area increases the surface energy density decreases. In any real application of the theory developed here $\eta$ is small but non-zero. The equations derived here are valid for small $\eta$ provided that the total surface energy density is of the order of the bulk energy or smaller and that the anchoring on each individual particle is weak enough not to induce defects.

In order to represent arbitrary particles undergoing rotational motion correctly within the homogenization scheme we use the level set method [5, 14, 38, 29, 9] to compute the expansion of the unit normal vector and the value of the term $\hat{\boldsymbol{n}} \cdot \frac{\partial \boldsymbol{r}_{\boldsymbol{x}}}{\partial \psi}$ in equation (2.31). We express the location of the particle surface as a level set $\chi_{LS}(\psi(\boldsymbol{x}), \boldsymbol{y}) = 0$ so that now the position vector of the particle boundary is a function of both $\boldsymbol{x}$ and $\boldsymbol{y}$, $\boldsymbol{r}(\boldsymbol{x}, \boldsymbol{y})$, and so are its perpendicular $\boldsymbol{r}_\perp = [-r_2, r_1]^T$, the particle boundary $\Gamma$ and the cell domain $\Omega$. The expansion of the unit normal is given by

$$\hat{\boldsymbol{n}} = \frac{\boldsymbol{\nabla}_{\boldsymbol{x}}\chi_{LS} + \frac{1}{\eta}\boldsymbol{\nabla}_{\boldsymbol{y}}\chi_{LS}}{|\boldsymbol{\nabla}_{\boldsymbol{x}}\chi_{LS} + \frac{1}{\eta}\boldsymbol{\nabla}_{\boldsymbol{y}}\chi_{LS}|} = \hat{\boldsymbol{n}}_0 + \eta\hat{\boldsymbol{n}}_1 + O(\eta^2) \tag{3.2}$$

where

$$\hat{\boldsymbol{n}}_0 = \frac{\boldsymbol{\nabla}_{\boldsymbol{y}}\chi_{LS}}{|\boldsymbol{\nabla}_{\boldsymbol{y}}\chi_{LS}|}, \tag{3.3a}$$

$$\hat{\boldsymbol{n}}_1 = \frac{\boldsymbol{\nabla}_{\boldsymbol{x}}\chi_{LS}}{|\boldsymbol{\nabla}_{\boldsymbol{y}}\chi_{LS}|} - \hat{\boldsymbol{n}}_0 \frac{\hat{\boldsymbol{n}}_0 \cdot \boldsymbol{\nabla}_{\boldsymbol{x}}\chi_{LS}}{|\boldsymbol{\nabla}_{\boldsymbol{y}}\chi_{LS}|}. \tag{3.3b}$$

There is a corresponding expansion for the tangent vector $\hat{\boldsymbol{t}} \equiv [-n_2, n_1]^T$:

$$\hat{\boldsymbol{t}} = \boldsymbol{t}_0 + \eta\boldsymbol{t}_1, \tag{3.4}$$

where $\boldsymbol{t}_j = [-n_2^{(j)}, n_1^{(j)}]^T$, with $\boldsymbol{n}_j = [n_1^{(j)}, n_2^{(j)}]^T$.

We now determine the "speed" of the boundary i.e. $\frac{\partial \boldsymbol{r}}{\partial \psi}$. As mentioned in section 2.4, $\boldsymbol{r}$ is the position vector of a point on the surface of a given particle. In the context of homogenization, $\boldsymbol{r}$ is a rapidly varying quantity and hence a function of

the $\boldsymbol{y}$ coordinates. We can therefore use the implicit function theorem on the level set definition of the particle boundary to obtain

$$\frac{\partial r_i}{\partial \psi} = -\frac{\partial \chi_{LS}}{\partial \psi}\left(\frac{\partial \chi_{LS}}{\partial y_i}\right)^{-1}. \tag{3.5}$$

By utilizing the following symmetry of $\chi_{LS}$ in its two arguments

$$\chi_{LS}(0, R^T(\psi(\boldsymbol{x}))\boldsymbol{y}) = \chi_{LS}(\psi(\boldsymbol{x}), \boldsymbol{y}) \tag{3.6}$$

and using the chain rule we find

$$\frac{\partial \chi_{LS}}{\partial \psi} = -\boldsymbol{r}_{\boldsymbol{x}\perp} \cdot \boldsymbol{\nabla}_{\boldsymbol{y}} \chi_{LS}. \tag{3.7}$$

Hence

$$\frac{\partial \boldsymbol{r}}{\partial \psi} \cdot \hat{\boldsymbol{n}}_0 = \boldsymbol{r}_{\boldsymbol{x}\perp} \cdot \hat{\boldsymbol{n}}_0. \tag{3.8}$$

**3.2. Scaling of equations.** As the size of the particles decreases so does the magnitude of the torques on the particles. To make the analysis as transparent as possible we make the $\eta$ dependence of the terms in (2.31) explicit. This amounts to mapping the domain of integration from a domain with linear dimensions that scale with $\eta$ to a fixed cell domain of size one. As a consequence, the line element and position vector on the particle both scale linearly with $\eta$, surface elements scale with $\eta^2$ and the curvature scales as $\frac{1}{\eta}$. We define $dl = dl_{\boldsymbol{x}}/\eta$ the line element in the $\boldsymbol{y}$ coordinate and $\kappa = \eta\kappa_{\boldsymbol{x}}$ the scaled curvature. With these scalings the particle governing equation [cfr. (2.31)] is

$$\begin{aligned}
&\eta^2 \int_\Gamma \boldsymbol{r}_\perp \cdot (-p\hat{\boldsymbol{n}} + \zeta' \mathcal{D}\hat{\boldsymbol{n}})\, dl \\
&\qquad + \eta^2 \int_\Gamma \left\{ \boldsymbol{r}_\perp \cdot \hat{\boldsymbol{n}} \left[ (\mathcal{W}\boldsymbol{a}) \cdot \left( \frac{\partial \boldsymbol{a}}{\partial t} + \boldsymbol{v} \cdot \boldsymbol{\nabla}\boldsymbol{a} \right) \right] + 2|\boldsymbol{a}|^2 \boldsymbol{r}_\perp \cdot (W\hat{\boldsymbol{n}}) \right\} dl \\
&\qquad = -\eta^2 \int_\Gamma \left( \frac{\xi_0^2}{2} \|\boldsymbol{\nabla}\boldsymbol{a}\|^2 - \frac{1}{2}|\boldsymbol{a}|^2 + \frac{1}{4}|\boldsymbol{a}|^4 \right) \left( \hat{\boldsymbol{n}} \cdot \frac{\partial \boldsymbol{r}}{\partial \psi} \right) dl \\
&\qquad - \eta^2 \beta_1 \int_\Gamma \left[ (\boldsymbol{a}_S - \boldsymbol{a}) \cdot \boldsymbol{a}_{S\perp} + \eta^2 \frac{\beta_1}{\xi_0^2} (\hat{\boldsymbol{n}} \cdot \boldsymbol{r}_\perp) |\boldsymbol{a}_S - \boldsymbol{a}|^2 \right. \\
&\qquad\qquad \left. + \frac{\kappa_{\boldsymbol{x}}}{2} (\hat{\boldsymbol{n}} \cdot \boldsymbol{r}_\perp) |\boldsymbol{a}_S - \boldsymbol{a}|^2 \right] dl \\
&\qquad - \eta^2 \chi_u \int_\Gamma r_\perp \cdot (\hat{\boldsymbol{n}} \cdot T_M)\, dl,
\end{aligned} \tag{3.9}$$

where $\boldsymbol{a}_{S\perp} = -2\mathcal{W}\boldsymbol{a}_S$. The fluid flow obeys [cfr. (2.29)]

$$\frac{\zeta'}{2}\nabla^2 \boldsymbol{v} = \boldsymbol{\nabla} p + \xi_0^2 \boldsymbol{\nabla} \cdot (\boldsymbol{\nabla}\boldsymbol{a} \cdot \boldsymbol{\nabla}\boldsymbol{a}) - \mathcal{W}\boldsymbol{\nabla}(\boldsymbol{a}\mathcal{W}\mathring{\boldsymbol{a}}), \qquad \boldsymbol{x} \in \mathrm{D}, \tag{3.10a}$$

$$\boldsymbol{\nabla} \cdot \boldsymbol{v} = 0, \qquad \boldsymbol{x} \in \mathrm{D}, \tag{3.10b}$$

$$\boldsymbol{v} = \eta \frac{\partial \psi}{\partial t} \boldsymbol{r}_\perp, \qquad \boldsymbol{x} \in \mathcal{B}_{\mathrm{D}}, \tag{3.10c}$$

$$\boldsymbol{v} = 0, \qquad \boldsymbol{x} \in \mathcal{O}_{\mathrm{D}}. \tag{3.10d}$$

while the nematic dynamics is determined by [cfr. (2.25)]

$$\mathring{\boldsymbol{a}} = \xi_0^2 \nabla^2 \boldsymbol{a} + \chi_a \boldsymbol{e} + \boldsymbol{a} - \boldsymbol{a}|\boldsymbol{a}|^2 \qquad \boldsymbol{x} \in \mathrm{D}, \tag{3.11a}$$

$$\hat{\boldsymbol{n}} \cdot \boldsymbol{\nabla} \boldsymbol{a} = \eta W_A^{(1)} \left( \boldsymbol{a}_S - \boldsymbol{a} \right), \qquad \boldsymbol{x} \in \mathcal{B}_\mathrm{D}, \tag{3.11b}$$

$$\boldsymbol{a} = \boldsymbol{b}(\boldsymbol{x}), \qquad \boldsymbol{x} \in \mathcal{O}_\mathrm{D}. \tag{3.11c}$$

The equation governing the electrostatic potential (2.32) is unchanged.

At this point there are two possible approaches we could follow in order to derive the appropriate homogenized equations. The first is the method of formal asymptotic expansions, see for example [33]. The second is the two-scale convergence method [31, 2]. Whilst the latter is mathematically rigorous, the former is based around a regular asymptotic expansion which has the advantage of increasing the clarity of the derivation. Hence, in this work, we will derive the homogenized equations using the formal asymptotic expansion method. This consists in expanding all equations and collecting terms at each order. In order to make the derivation of the macroscopic equations clearer, here we follow a slightly different approach: we first solve the drag equation to eliminate the fluid velocity and then analyze the particle–liquid crystal equations. Solving the drag equations will allow us to show that the fluid velocity effectively decouples from the director alignment. We will carry out this step in the next subsection and then move on to homogenize the remaining equations.

**3.3. Expanding the drag.** As mentioned in section 3.1, in this paper we take a double limit of the microscopic equations, namely $\eta \to 0$ and $\xi_0^2 \to 0$. In the case of the velocity equations the latter limit is regular and we take it immediately, thus reducing equations (3.10) to

$$\frac{\zeta'}{2} \nabla^2 \boldsymbol{v} = \boldsymbol{\nabla} p - \mathcal{W} \boldsymbol{\nabla} (\boldsymbol{a} \mathcal{W} \mathring{\boldsymbol{a}}), \qquad \boldsymbol{x} \in \mathrm{D}, \tag{3.12a}$$

$$\boldsymbol{\nabla} \cdot \boldsymbol{v} = 0, \qquad \boldsymbol{x} \in \mathrm{D}, \tag{3.12b}$$

$$\boldsymbol{v} = \eta \frac{\partial \psi}{\partial t} \boldsymbol{r}_\perp, \qquad \boldsymbol{x} \in \mathcal{B}_\mathrm{D}, \tag{3.12c}$$

$$\boldsymbol{v} = 0, \qquad \boldsymbol{x} \in \mathcal{O}_\mathrm{D}. \tag{3.12d}$$

We note that, by assumption, the fluid flow is coupled only to the particle orientation. Dealing with the fluid flow will then allow us to simplify (3.9) and determine an explicit set of equations for the particle motion. We make the usual expansions of the

gradient (3.1), the Laplacian and fields,

$$\nabla^2 = \nabla^2_{\boldsymbol{x}} + \frac{2}{\eta}\boldsymbol{\nabla}_{\boldsymbol{x}} \cdot \boldsymbol{\nabla}_{\boldsymbol{y}} + \frac{1}{\eta^2}\nabla^2_{\boldsymbol{y}}, \tag{3.13a}$$

$$\boldsymbol{v} = \boldsymbol{v}_0 + \eta \boldsymbol{v}_1 + \eta^2 \boldsymbol{v}_2, \tag{3.13b}$$

$$\mathcal{D} = \frac{1}{\eta}\mathcal{D}^{(-1)} + \mathcal{D}^{(0)} + \eta\mathcal{D}^{(1)}, \tag{3.13c}$$

$$W = \frac{1}{\eta}W^{(-1)} + W^{(0)} + \eta W^{(1)}, \tag{3.13d}$$

$$p = p_0 + \eta p_1 + \eta^2 p_2, \tag{3.13e}$$

$$\boldsymbol{a} = \boldsymbol{a}_0 + \eta \boldsymbol{a}_1 + \eta^2 \boldsymbol{a}_2, \tag{3.13f}$$

$$\phi = \phi_0 + \eta\phi_1 + \eta^2\phi_2, \tag{3.13g}$$

$$\boldsymbol{e} = \frac{1}{\eta^2}\boldsymbol{e}_{-2} + \frac{1}{\eta}\boldsymbol{e}_{-1} + \boldsymbol{e}_0, \tag{3.13h}$$

$$\mathcal{Q} = \mathcal{Q}^{(0)} + \eta\mathcal{Q}^{(1)} + \eta^2\mathcal{Q}^{(2)}. \tag{3.13i}$$

$W^{(k)}$ and $\mathcal{D}^{(k)}$, $k = -1, 0, 1, \ldots$, are defined by equations (2.10-2.11) respectively in terms of the derivatives of the expansion of the velocity $\boldsymbol{v}$. For example,

$$W^{(-1)}_{ij} = \frac{1}{2}\left(\frac{\partial v_{0i}}{\partial y_j} - \frac{\partial v_{0j}}{\partial y_i}\right). \tag{3.14}$$

$\mathcal{Q}^{(k)} = \sum_{i=1}^{2} a_i^{(k)}\mathcal{T}^{(i)}$, with $\boldsymbol{a}_k = (a_1^{(k)}, a_2^{(k)})$, $k = 0, 1, 2$. The expansion for the electric field tensor components $\boldsymbol{e}$ in equation (3.13h) is obtained by substituting equations (3.1) and (3.13g) together with the relation $\boldsymbol{E} = -\boldsymbol{\nabla}\phi$ in equation (2.18) and projecting on the basis (2.3) of traceless symmetric tensors. For example, the $k$-th component of $\boldsymbol{e}_{-2}$ is

$$\begin{aligned} e_k^{(-2)} &= \sqrt{2}\mathrm{Tr}\left[\left(\boldsymbol{\nabla}_{\boldsymbol{y}}\phi_0 \otimes \boldsymbol{\nabla}_{\boldsymbol{y}}\phi_0 - \frac{1}{2}\mathcal{I}\,|\boldsymbol{\nabla}_{\boldsymbol{y}}\phi_0|^2\right)\mathcal{T}^{(k)}\right] \\ &= \sqrt{2}\mathrm{Tr}\left[\left(\boldsymbol{\nabla}_{\boldsymbol{y}}\phi_0 \otimes \boldsymbol{\nabla}_{\boldsymbol{y}}\phi_0\right)\mathcal{T}^{(k)}\right]. \end{aligned} \tag{3.15}$$

Substituting equations (3.13) into Stokes' equation (3.12) we obtain a sequence of problems at different orders in $\eta$. Solving these in ascending powers of $\eta$ we will derive the cell problem for the fluid flow and use the result to simplify the drag term, i.e. the first integral on the left-hand side of equation (3.9), namely

$$F = \int_\Gamma \boldsymbol{r}_\perp \cdot (-p\hat{\boldsymbol{n}} + \zeta'\mathcal{D}\hat{\boldsymbol{n}})\, dl. \tag{3.16}$$

**3.3.1. Leading order.** We will show in section 3.4.1 that the leading order term of the director field components, $\boldsymbol{a}_0$, is a function of the macroscopic variables only, $\boldsymbol{a}_0(\boldsymbol{x}, t)$. Therefore, the leading order expansion of the fluid equation (3.15) is

$$\boldsymbol{\nabla}^2_{\boldsymbol{y}}\boldsymbol{v}_0 = 0, \qquad \boldsymbol{y} \in \Omega, \tag{3.17a}$$

$$\boldsymbol{\nabla}_{\boldsymbol{y}} \cdot \boldsymbol{v}_0 = 0, \qquad \boldsymbol{y} \in \Omega, \tag{3.17b}$$

$$\boldsymbol{v}_0 = \boldsymbol{0}, \qquad \boldsymbol{y} \in \Gamma. \tag{3.17c}$$

subject to a periodic boundary condition on $\partial\hat{\Omega}$, the outer cell walls. In the derivation of equation (3.17a) we have used the incompressibility condition (3.17b), the definition (2.20) of corotational derivative and the fact that $\boldsymbol{a}_0$ does not depend on $\boldsymbol{y}$ to simplify the term $\mathcal{W}\boldsymbol{\nabla}_{\boldsymbol{y}}(\boldsymbol{a}_0\mathcal{W}\mathring{\boldsymbol{a}}_0)$ in the lowest order expansion of equation (3.12a) to $\boldsymbol{\nabla}^2_{\boldsymbol{y}}\boldsymbol{v}_0$. Equations (3.17) have solution $\boldsymbol{v}_0 = 0$. Hence, $\mathcal{D}^{(-1)} = 0$.

**3.3.2. First order.** At this order the fluid obeys

$$\frac{\zeta'}{2}\nabla^2_{\boldsymbol{y}}\boldsymbol{v}_1 = \boldsymbol{\nabla}_{\boldsymbol{y}}p_0 + 2\boldsymbol{\nabla}_{\boldsymbol{y}}\cdot W^{(0)}|\boldsymbol{a}_0|^2, \qquad \boldsymbol{y}\in\Omega, \tag{3.18a}$$

$$\boldsymbol{\nabla}_{\boldsymbol{y}}\cdot\boldsymbol{v}_1 = 0, \qquad \boldsymbol{y}\in\Omega, \tag{3.18b}$$

$$\boldsymbol{v}_1 = \frac{\partial\psi}{\partial t}\boldsymbol{r}_\perp, \qquad \boldsymbol{y}\in\Gamma, \tag{3.18c}$$

subject to periodic boundary conditions on $\partial\hat{\Omega}_j$. As the fluid is driven by the particle rotation through the boundary condition (3.18c), we make the ansatz $\boldsymbol{v}_1 = \boldsymbol{u}_1\frac{\partial\psi}{\partial t}$ and $p_0 = P_0\frac{\partial\psi}{\partial t}$, where both $P_0$ and $\boldsymbol{u}_1$ depend on $\boldsymbol{y}$. The system of equations for $\boldsymbol{u}_1$ is

$$\left[\frac{\zeta'}{2} + |\boldsymbol{a}_0|^2\right]\nabla^2_{\boldsymbol{y}}\boldsymbol{u}_1 = \boldsymbol{\nabla}_{\boldsymbol{y}}P_0, \qquad \boldsymbol{y}\in\Omega, \tag{3.19a}$$

$$\boldsymbol{\nabla}_{\boldsymbol{y}}\cdot\boldsymbol{u}_1 = 0, \qquad \boldsymbol{y}\in\Omega, \tag{3.19b}$$

$$\boldsymbol{u}_1 = \boldsymbol{r}_\perp, \qquad \boldsymbol{y}\in\Gamma. \tag{3.19c}$$

Equations (3.19) are the cell problem for $\boldsymbol{u}_1$ and can be solved numerically. It should be noted that, in the absence of defects, $|\boldsymbol{a}_0|^2$ is constant with respect to $\boldsymbol{y}$. Hence, its effect is just to scale locally the viscosity. The order $\eta^0$ term of the symmetric part of the velocity gradient is given by

$$\mathcal{D}^{(0)} = \frac{1}{2}\left[\boldsymbol{\nabla}_{\boldsymbol{y}}\boldsymbol{v}_1 + (\boldsymbol{\nabla}_{\boldsymbol{y}}\boldsymbol{v}_1)^T\right]. \tag{3.20}$$

and the Stokes' drag component of the net drag on a particle, equation (3.16), can be expanded as

$$\int_\Gamma \boldsymbol{r}_\perp\cdot\left(\zeta'\mathcal{D}^{(0)}\hat{\boldsymbol{n}}_0 - \hat{\boldsymbol{n}}_0 p_0\right)dl = \frac{\partial\psi}{\partial t}\int_\Gamma \boldsymbol{r}_\perp\cdot\left(\zeta'\mathcal{D}^{(0)\prime}\hat{\boldsymbol{n}}_0 - \hat{\boldsymbol{n}}_0 P_0\right)dl + \mathcal{O}(\eta). \tag{3.21}$$

where

$$\mathcal{D}^{(0)\prime} = \frac{1}{2}\left[\boldsymbol{\nabla}_{\boldsymbol{y}}\boldsymbol{u}_1 + (\boldsymbol{\nabla}_{\boldsymbol{y}}\boldsymbol{u}_1)^T\right]. \tag{3.22}$$

Using equation (3.21) we simplify the particle equation (3.9) to

$$\begin{aligned}
&\kappa_0'\frac{\partial\psi}{\partial t} + \int_\Gamma\left\{\boldsymbol{r}_\perp\cdot\hat{\boldsymbol{n}}\left[(\mathcal{W}\boldsymbol{a})\cdot\left(\frac{\partial\boldsymbol{a}}{\partial t} + \boldsymbol{v}\cdot\boldsymbol{\nabla}\boldsymbol{a}\right)\right] + 2|\boldsymbol{a}|^2\boldsymbol{r}_\perp\cdot(W\hat{\boldsymbol{n}})\right\}dl = \\
&-\int_\Gamma\left(\frac{\xi_0^2}{2}\|\boldsymbol{\nabla}\boldsymbol{a}\|^2 - \frac{1}{2}|\boldsymbol{a}|^2 + \frac{1}{4}|\boldsymbol{a}|^4\right)\left(\hat{\boldsymbol{n}}\cdot\frac{\partial\boldsymbol{r}}{\partial\psi}\right)dl \\
&-\beta_1\int_\Gamma\left[(\boldsymbol{a}_S - \boldsymbol{a})\cdot\boldsymbol{a}_{S\perp} + \eta^2 W(\hat{\boldsymbol{n}}\cdot\boldsymbol{r}_\perp)|\boldsymbol{a}_S - \boldsymbol{a}|^2 + \frac{\kappa}{2}(\hat{\boldsymbol{n}}\cdot\boldsymbol{r}_\perp)|\boldsymbol{a}_S - \boldsymbol{a}|^2\right]dl \\
&-\chi_u\int_\Gamma \boldsymbol{r}_\perp\cdot(\hat{\boldsymbol{n}}\cdot T_M)\,dl,
\end{aligned} \tag{3.23}$$

where the time constant in equation (3.23) is given by

$$\kappa_0' = \int_\Gamma \boldsymbol{r}_\perp \cdot \left(\zeta' \mathcal{D}^{(0)\prime} \hat{\boldsymbol{n}}_0 - \hat{\boldsymbol{n}}_0 P_0\right) dl. \tag{3.24}$$

As we are only interested in the leading order time dynamics of $\psi$ we do not consider higher order terms in the expansion of the drag equations. We will complete the expansion of equation (3.23) at the end of the next section, once we have completed the expansion of the director and electric fields.

**3.4. Nematic dynamics and the electric field.** Having obtain a simplified equation for the particles (3.23), we now proceed to homogenize equations (2.32) and (3.11). As in the previous section, we expand derivatives and all the fields, equations (3.1) and (3.13).

**3.4.1. Leading order.** At leading order the nematic equations (3.11) are

$$\xi_0^2 \nabla_{\boldsymbol{y}}^2 \boldsymbol{a}_0 + \chi_a \boldsymbol{e}_{-2} = 0, \qquad \boldsymbol{y} \in \Omega, \tag{3.25a}$$

$$\hat{\boldsymbol{n}}_0 \cdot \boldsymbol{\nabla}_{\boldsymbol{y}} \boldsymbol{a}_0 = 0, \qquad \boldsymbol{y} \in \Gamma, \tag{3.25b}$$

subject to periodic boundary conditions on the outer boundaries of the unit cell. Similarly, the leading order expansion of Maxwell's equation for the electric potential is

$$\boldsymbol{\nabla}_{\boldsymbol{y}} \cdot \left[\left(\mathcal{I} + \alpha \mathcal{Q}^{(0)}\right) \boldsymbol{\nabla}_{\boldsymbol{y}} \phi_0\right] = 0, \qquad \boldsymbol{y} \in \Omega, \tag{3.26a}$$

$$\boldsymbol{t}_0 \cdot \boldsymbol{\nabla}_{\boldsymbol{y}} \phi_0 = 0, \qquad \boldsymbol{y} \in \Gamma, \tag{3.26b}$$

$$\int_\Gamma \left[\left(\mathcal{I} + \alpha \mathcal{Q}^{(0)}\right) \boldsymbol{\nabla}_{\boldsymbol{y}} \phi_0\right] \cdot \hat{\boldsymbol{n}}_0 \, dl = 0, \tag{3.26c}$$

with periodic boundary conditions on $\partial\hat{\Omega}$. The solution of equations (3.25, 3.26) is $\boldsymbol{a}_0 = \boldsymbol{a}_0(\boldsymbol{x})$ and $\phi_0 = \phi_0(\boldsymbol{x})$.

**3.4.2. First order correction.** At order $\mathcal{O}(\eta)$ we find that for each cell

$$\xi_0^2 \nabla_{\boldsymbol{y}}^2 \boldsymbol{a}_1 = 0, \qquad \boldsymbol{y} \in \Omega, \tag{3.27a}$$

$$\hat{\boldsymbol{n}}_0 \cdot \boldsymbol{\nabla}_y \boldsymbol{a}_1 + \hat{\boldsymbol{n}}_0 \cdot \boldsymbol{\nabla}_x \boldsymbol{a}_0 = 0, \qquad \boldsymbol{y} \in \Gamma. \tag{3.27b}$$

No $\boldsymbol{e}_{-1}$ term is present in equation (3.27a) because the electric field tensor $\mathcal{E}$, defined in equation (2.18), is quadratic in the gradient of the potential and $\boldsymbol{\nabla}_{\boldsymbol{y}} \phi_0 = \boldsymbol{0}$. Equation (3.27) is equivalent to the standard order one problem for diffusion of solutes in porous media [23], hence solvability is guaranteed. As the $\boldsymbol{x}$ dependence in this equation is only through a single term in the boundary condition (3.27b), we can scale it out by writing the solution as $\boldsymbol{a}_1 = \chi_k \frac{\partial \boldsymbol{a}_0}{\partial x_k}$. Substituting into equations (3.27) we obtain the cell problem for $\chi_k$, $k = 1, 2$,

$$\nabla_{\boldsymbol{y}}^2 \chi_k = 0, \qquad \boldsymbol{y} \in \Omega, \tag{3.28a}$$

$$\hat{\boldsymbol{n}}_0 \cdot \boldsymbol{\nabla}_{\boldsymbol{y}} \chi_k = -\hat{\boldsymbol{n}}_0 \cdot \hat{\boldsymbol{e}}_k, \qquad \boldsymbol{y} \in \Gamma. \tag{3.28b}$$

Here $\hat{\boldsymbol{e}}_k$ is the $k$-th coordinate unit vector. These equations (with periodic boundary conditions) define $\chi_k$ up to a constant (with respect to $\boldsymbol{y}$). Hence we can write

$$\boldsymbol{a}_1 = \chi_k \frac{\partial \boldsymbol{a}_0}{\partial x_k} + \overline{\boldsymbol{a}}_1(\boldsymbol{x}), \tag{3.29}$$

where $\overline{\boldsymbol{a}}_1(\boldsymbol{x})$ is undetermined at this order and will not be needed in the derivation of the macroscopic equations.

The first order terms of the expansion of Maxwell's equation are

$$\boldsymbol{\nabla}_{\boldsymbol{y}} \cdot \left[ \left( \mathcal{I} + \alpha \mathcal{Q}^{(0)} \right) \boldsymbol{\nabla}_{\boldsymbol{y}} \phi_1 \right] = 0, \qquad \boldsymbol{y} \in \Omega, \tag{3.30a}$$

$$\boldsymbol{t}_0 \cdot (\boldsymbol{\nabla}_x \phi_0 + \boldsymbol{\nabla}_{\boldsymbol{y}} \phi_1) = 0, \qquad \boldsymbol{y} \in \Gamma, \tag{3.30b}$$

$$\int_\Gamma \left[ \hat{\boldsymbol{n}}_0 \cdot \left( \mathcal{I} + \alpha \mathcal{Q}^{(0)} \right) (\boldsymbol{\nabla}_{\boldsymbol{y}} \phi_1 + \boldsymbol{\nabla}_{\boldsymbol{x}} \phi_0) \right] dl = 0. \tag{3.30c}$$

Here $\mathcal{Q}^{(0)}$ is the order $\mathcal{O}(\eta^0)$ part of the $\mathcal{Q}$-tensor and has component vector $\boldsymbol{a}_0$. This equation satisfies a solvability condition. An easy way to check this is to integrate (3.30a) over $\Omega$ and use the divergence theorem and condition (3.30c). The cell problem for the electric field is derived by making the ansatz, similar to equation (3.29),

$$\phi_1 = \sum_{k=1}^{2} R_k(\boldsymbol{x}, \boldsymbol{y}) \frac{\partial \phi_0}{\partial x_k} + \bar{\phi}_1(\boldsymbol{x}). \tag{3.31}$$

By substituting this ansatz into equations (3.30) we find

$$\left( \delta_{nm} + \alpha \mathcal{Q}^{(0)}_{nm} \right) \frac{\partial^2 R_k}{\partial y_n \partial y_m} = 0, \qquad \boldsymbol{y} \in \Omega, \tag{3.32a}$$

$$(\boldsymbol{t}_0 \cdot \boldsymbol{\nabla}_{\boldsymbol{y}}) R_k = -\boldsymbol{t}_0 \cdot \hat{\boldsymbol{e}}_k, \qquad \boldsymbol{y} \in \Gamma, \tag{3.32b}$$

$$\int_\Gamma \hat{\boldsymbol{n}}_0 \cdot \left( \mathcal{I} + \alpha \mathcal{Q}^{(0)} \right) \boldsymbol{\nabla}_{\boldsymbol{y}} R_k(\boldsymbol{y}) \, dl = 0, \tag{3.32c}$$

which must be solved numerically for varying particle orientations and realizations of $\mathcal{Q}^{(0)}$.

**3.4.3. Homogenization.** At order $\mathcal{O}(\eta^0)$ the nematic equations give

$$\mathring{\boldsymbol{a}}_0 = \xi_0^2 \left( \nabla^2_{\boldsymbol{x}} \boldsymbol{a}_0 + 2 \boldsymbol{\nabla}_{\boldsymbol{x}} \cdot \boldsymbol{\nabla}_{\boldsymbol{y}} \boldsymbol{a}_1 + \nabla^2_{\boldsymbol{y}} \boldsymbol{a}_2 \right) + \boldsymbol{a}_0 - \boldsymbol{a}_0 |\boldsymbol{a}_0|^2 + \chi_a \boldsymbol{e}_0, \qquad \boldsymbol{y} \in \Omega, \tag{3.33a}$$

$$\hat{\boldsymbol{n}}_0 \cdot (\boldsymbol{\nabla}_{\boldsymbol{y}} \boldsymbol{a}_2 + \boldsymbol{\nabla}_{\boldsymbol{x}} \boldsymbol{a}_1) + \boldsymbol{n}_1 \cdot (\boldsymbol{\nabla}_{\boldsymbol{x}} \boldsymbol{a}_0 + \boldsymbol{n}_1 \cdot \boldsymbol{\nabla}_{\boldsymbol{y}} \boldsymbol{a}_1) = W_A^{(1)} (\boldsymbol{a}_S - \boldsymbol{a}_0), \qquad \boldsymbol{y} \in \Gamma. \tag{3.33b}$$

Once again we have to impose that this equation is solvable. As in the case of equation (3.30) we integrate (3.33a) over $\Omega$, and apply the divergence theorem and the boundary condition (3.33b). We find that equation (3.33) is solvable if

$$\begin{aligned} &\frac{1}{|\Omega|} \int_\Omega \left( \frac{\partial \boldsymbol{a}_0}{\partial t} - 2 W^{(0)} \boldsymbol{a}_0 \right) dS = \\ &\frac{\xi_0^2}{|\Omega|} \int_\Omega \boldsymbol{\nabla}_{\boldsymbol{x}} \cdot (\boldsymbol{\nabla}_{\boldsymbol{x}} \boldsymbol{a}_0 + \boldsymbol{\nabla}_{\boldsymbol{y}} \boldsymbol{a}_1) \, dS + \boldsymbol{a}_0 - \boldsymbol{a}_0 |\boldsymbol{a}_0|^2 \\ &+ \chi_a \frac{1}{|\Omega|} \int_\Omega \boldsymbol{e}_0 \, dS + \frac{\beta_1}{|\Omega|} \int_\Gamma (\boldsymbol{a}_S - \boldsymbol{a}_0) \, dl - \frac{\xi_0^2}{|\Omega|} \int_\Gamma \boldsymbol{n}_1 \cdot (\boldsymbol{\nabla}_{\boldsymbol{x}} \boldsymbol{a}_0 + \boldsymbol{\nabla}_{\boldsymbol{y}} \boldsymbol{a}_1) \, dl, \end{aligned} \tag{3.34}$$

where $|\Omega|$ is the area of $\Omega$ and $W^{(0)}$ is the order zero term of the vorticity expansion, (3.13d). We now simplify the left hand-side of equation (3.34). Using equations (3.19) and the divergence theorem we find

$$\frac{1}{|\Omega|}\int_\Omega \left(\frac{\partial \boldsymbol{a}_0}{\partial t} - 2W^{(0)}\boldsymbol{a}_0\right) dS = \frac{\partial \boldsymbol{a}_0}{\partial t} - \frac{2}{|\Omega|}\frac{\partial \psi}{\partial t}\boldsymbol{a}_\perp. \tag{3.35}$$

Next we use the transport theorem on the first integral on the right hand side

$$\begin{aligned}\boldsymbol{\nabla}_{\boldsymbol{x}} \cdot \int_\Omega \left(\boldsymbol{\nabla}_{\boldsymbol{x}}\boldsymbol{a}_0 + \boldsymbol{\nabla}_{\boldsymbol{y}}\boldsymbol{a}_1\right) dS = &\int_\Omega \boldsymbol{\nabla}_{\boldsymbol{x}} \cdot \left(\boldsymbol{\nabla}_{\boldsymbol{x}}\boldsymbol{a}_0 + \boldsymbol{\nabla}_{\boldsymbol{y}}\boldsymbol{a}_1\right) dS \\ &+ \int_\Gamma \left(\boldsymbol{\nabla}_{\boldsymbol{x}}\boldsymbol{a}_0 + \boldsymbol{\nabla}_{\boldsymbol{y}}\boldsymbol{a}_1\right) \cdot \left(\boldsymbol{\nabla}_{\boldsymbol{x}}\boldsymbol{r} \cdot \hat{\boldsymbol{n}}_0\right) dl,\end{aligned} \tag{3.36}$$

and we use the level set representation to write

$$\boldsymbol{\nabla}_{\boldsymbol{x}}\boldsymbol{r} \cdot \hat{\boldsymbol{n}}_0 = -\frac{\boldsymbol{\nabla}_{\boldsymbol{x}}\chi_{LS}}{\|\boldsymbol{\nabla}_{\boldsymbol{y}}\chi_{LS}\|}. \tag{3.37}$$

Hence,

$$\begin{aligned}\int_\Omega \boldsymbol{\nabla}_{\boldsymbol{x}} \cdot \left(\boldsymbol{\nabla}_{\boldsymbol{x}}\boldsymbol{a}_0 + \boldsymbol{\nabla}_{\boldsymbol{y}}\boldsymbol{a}_1\right) dS = &\boldsymbol{\nabla}_{\boldsymbol{x}} \cdot \int_\Omega \left(\boldsymbol{\nabla}_{\boldsymbol{x}}\boldsymbol{a}_0 + \boldsymbol{\nabla}_{\boldsymbol{y}}\boldsymbol{a}_1\right) dS \\ &+ \int_\Gamma \left(\boldsymbol{\nabla}_{\boldsymbol{x}}\boldsymbol{a}_0 + \boldsymbol{\nabla}_{\boldsymbol{y}}\boldsymbol{a}_1\right) \cdot \frac{\boldsymbol{\nabla}_{\boldsymbol{x}}\chi_{LS}}{\|\boldsymbol{\nabla}_{\boldsymbol{y}}\chi_{LS}\|}\, dl\,.\end{aligned} \tag{3.38}$$

In addition, using boundary condition (3.27b) we see that on $\Gamma$

$$\boldsymbol{n}_1 \cdot \left(\boldsymbol{\nabla}_{\boldsymbol{x}}\boldsymbol{a}_0 + \boldsymbol{\nabla}_{\boldsymbol{y}}\boldsymbol{a}_1\right) = \frac{\boldsymbol{\nabla}_{\boldsymbol{x}}\chi_{LS}}{\|\boldsymbol{\nabla}_{\boldsymbol{y}}\chi_{LS}\|} \cdot \left(\boldsymbol{\nabla}_{\boldsymbol{x}}\boldsymbol{a}_0 + \boldsymbol{\nabla}_{\boldsymbol{y}}\boldsymbol{a}_1\right). \tag{3.39}$$

Substituting equations (3.38), (3.39) into (3.34) we obtain the macroscopic equation for the liquid crystal alignment:

$$\begin{aligned}\frac{\partial \boldsymbol{a}_0}{\partial t} - \frac{2}{|\Omega|}\frac{\partial \psi}{\partial t}\boldsymbol{a}_\perp = &\xi_0^2 \boldsymbol{\nabla}_{\boldsymbol{x}} \cdot \mathcal{K}\boldsymbol{\nabla}_{\boldsymbol{x}}\boldsymbol{a}_0 + \boldsymbol{a}_0 - \boldsymbol{a}_0|\boldsymbol{a}_0|^2 \\ &+ \chi_a\left[\boldsymbol{e}_M\left(1 + 2\frac{|\Omega_{\rm np}|}{|\Omega|}\right) + \boldsymbol{p}\right] + \frac{\beta_1}{|\Omega|}\int_{\Gamma(\boldsymbol{x})} \left(\boldsymbol{a}_S - \boldsymbol{a}_0\right) dl\,,\end{aligned} \tag{3.40}$$

where $\Omega_{\rm np}$ is the domain of a nanoparticle. This equation is valid for all $\boldsymbol{x} \in \mathrm{D}_H = [0, \ell] \times [0, 1]$, and we no longer need to consider the perforated microscopic domain D. We call $\mathrm{D}_H$ the *macroscopic* domain. The boundary conditions are given by equation (3.11c) written for $\boldsymbol{a}_0$,

$$\boldsymbol{a}_0 = \boldsymbol{b}(\boldsymbol{x}), \qquad \boldsymbol{x} \in \mathcal{O}_{\rm D}. \tag{3.41}$$

The new elasticity term is given by

$$\mathcal{K}_{ij} = \frac{1}{|\Omega|}\int_{\Omega(\boldsymbol{x})} \left(\delta_{ij} + \frac{\partial \chi_j}{\partial y_i}\right) dS, \tag{3.42}$$

the macroscopic electric field $\boldsymbol{e}_M$ has components given by

$$e_i^{(M)} = \sqrt{2}\mathrm{Tr}\left[\left(\boldsymbol{\nabla}_{\boldsymbol{x}}\phi_0 \otimes \boldsymbol{\nabla}_{\boldsymbol{x}}\phi_0\right)\mathcal{T}^{(i)}\right], \tag{3.43}$$

and the polarization components are

$$p_i = \frac{1}{|\Omega|}\int_\Omega \mathrm{Tr}\left(\sqrt{2}\boldsymbol{\nabla_y} R_k \otimes \boldsymbol{\nabla_y} R_l \phi_{0,k}\phi_{0,l}\mathcal{T}^{(i)}\right) dS. \tag{3.44}$$

The derivation of these last two terms is detailed in section SM2 of the Supplementary Material. Equation (3.40) is one of the key results of this paper and each of its terms gives insight to the physics of the colloidal suspension. However, we defer a discussion of their meaning to section 3.5 where we use the difference in scale between the various terms to simplify this equation further. Instead, now we derive the second macroscopic equation, namely that for the electrostatic field. At this order Maxwell's equation for the electric potential and its boundary condition are

$$\begin{aligned}&\boldsymbol{\nabla_y}\cdot[(\mathcal{I}+\alpha\mathcal{Q}^{(0)})(\boldsymbol{\nabla_y}\phi_2+\boldsymbol{\nabla_x}\phi_1)+\alpha\mathcal{Q}_1(\boldsymbol{\nabla_y}\phi_1+\boldsymbol{\nabla_x}\phi_0)],\\ &\quad+\boldsymbol{\nabla_x}\cdot[(\mathcal{I}+\alpha\mathcal{Q}^{(0)})(\boldsymbol{\nabla_x}\phi_0+\boldsymbol{\nabla_y}\phi_1)]=0, \qquad \boldsymbol{x}\in\Omega\end{aligned} \tag{3.45a}$$

$$\begin{aligned}&\int_\Gamma \hat{\boldsymbol{n}}_0\cdot\left[\left(\mathcal{I}+\alpha\mathcal{Q}^{(0)}\right)(\boldsymbol{\nabla_y}\phi_2+\boldsymbol{\nabla_x}\phi_1)+\alpha\mathcal{Q}_1(\boldsymbol{\nabla_y}\phi_1+\boldsymbol{\nabla_x}\phi_0)\right]dl\\ &+\int_\Gamma \boldsymbol{n}_o\cdot(\boldsymbol{y}\cdot\boldsymbol{\nabla_x})\left[\left(\mathcal{I}+\alpha\mathcal{Q}^{(0)}\right)(\boldsymbol{\nabla_x}\phi_0+\boldsymbol{\nabla_y}\phi_1)\right]dl\\ &+\int_\Gamma \boldsymbol{n}_1\cdot\left[\left(\mathcal{I}+\alpha\mathcal{Q}^{(0)}\right)(\boldsymbol{\nabla_x}\phi_0+\boldsymbol{\nabla_y}\phi_1)\right]dl=0,\end{aligned} \tag{3.45b}$$

where the second integral in the expansion (3.45b) of the boundary condition (3.30c) is due to the non-local nature of the integral constraint [13]. We have not written the expansion of the boundary condition (3.30b) because it is not needed for the derivation of the macroscopic equation for the potential. To impose the solvability condition we need to follow steps very similar to those leading from equation (3.33) to equation (3.40). Briefly, we integrate equation (3.45a) over $\Omega$, use the divergence theorem, apply the boundary condition (3.45b), the Reynolds transport theorem and some lengthy algebra based on equations (3.36)-(3.39), to obtain a macroscopic equation for the potential,

$$\boldsymbol{\nabla_x}\cdot[\mathrm{K}\boldsymbol{\nabla_x}\phi_0]=0, \qquad \boldsymbol{x}\in \mathrm{D}_H, \tag{3.46a}$$

$$\phi_0(\boldsymbol{x})=\Phi(\boldsymbol{x}), \qquad \boldsymbol{x}\in\mathcal{O}_\mathrm{D}, \tag{3.46b}$$

where

$$\mathrm{K}_{ij}=\delta_{ij}+\alpha\mathcal{Q}^{(0)}_{ij}+\int_{\partial\hat{\Omega}} y_i\boldsymbol{n}_0\cdot\left(\mathcal{I}+\alpha\mathcal{Q}^{(0)}\right)\boldsymbol{\nabla_x}R_j\,dl\,. \tag{3.47}$$

At leading order the electric field is

$$\boldsymbol{E}_0=-\boldsymbol{\nabla_x}\phi_0-\boldsymbol{\nabla_y}\phi_1. \tag{3.48}$$

As the last step in deriving a set of macroscopic equations, we simplify the particle equation (3.23). Using $\boldsymbol{a}_0=\boldsymbol{a}_0(\boldsymbol{x},t)$ and $\phi_0=\phi_0(\boldsymbol{x},t)$ we expand (3.23) to lowest order in $\eta$, namely $\eta^0$, and simplify the equation governing the particle dynamics considerably. The first term on the right hand side of equation (3.23) is the bulk elastic screening torque (see end of section 3.5 for a discussion of the physical meaning of this and the following torques). This becomes

$$\tau_B=-\xi_0^2\int_\Gamma\left[\frac{1}{2}\|\boldsymbol{\nabla_y}\boldsymbol{a}_1\|^2+\frac{1}{2}\|\boldsymbol{\nabla_x}\boldsymbol{a}_0\|^2+\boldsymbol{\nabla_x}\boldsymbol{a}_0:\boldsymbol{\nabla_y}\boldsymbol{a}_1\right](\hat{\boldsymbol{n}}_0\cdot\boldsymbol{r}_\perp)\,dl+\mathcal{O}(\eta). \tag{3.49}$$

The second term is the surface torque

$$\tau_S = \beta_1 \boldsymbol{a}_0 \cdot \int_\Gamma \left[\kappa(\hat{\boldsymbol{n}} \cdot \boldsymbol{r}_\perp)\mathcal{I} - 2\mathcal{W}\right] \boldsymbol{a}_S \, dl + \mathcal{O}(\eta). \tag{3.50}$$

The last term is the electric torque

$$\tau_E = -\chi_u \int_\Gamma \boldsymbol{r}_\perp \cdot \left(\hat{\boldsymbol{n}}_0 \cdot T_0^{(M)}\right) \, dl + \mathcal{O}(\eta), \tag{3.51}$$

where the first non-zero contribution from the Maxwell stress tensor is given by

$$T_0^{(M)} = \boldsymbol{E}_0 \otimes \boldsymbol{D}_0 - \frac{1}{2}(\boldsymbol{E}_0 \cdot \boldsymbol{D}_0)\mathcal{I}. \tag{3.52}$$

Here $\boldsymbol{E}_0$ is defined in equation (3.48) and $\boldsymbol{D}_0 = (\mathcal{I} + \alpha\mathcal{Q}^{(0)})\boldsymbol{E}_0$. They are the first non-zero contributions to the electric and displacement fields. Finally, we simplify the dynamic component of the viscous drag, the second term on the left hand side of equation (3.23). We expand it in powers of $\eta$, and use $\boldsymbol{v}_0 = 0$, $\boldsymbol{a}_0 = \boldsymbol{a}_0(\boldsymbol{x}, t)$ and the cell problem (3.19), to write it as

$$\begin{aligned} &\int_\Gamma \left\{ \boldsymbol{r}_\perp \cdot \hat{\boldsymbol{n}_0} \left[ (\mathcal{W}\boldsymbol{a}_0) \cdot \left( \frac{\partial \boldsymbol{a}_0}{\partial t} + \boldsymbol{v}_0 \cdot \boldsymbol{\nabla} \boldsymbol{a}_0 \right) \right] + 2|\boldsymbol{a}_0|^2 \boldsymbol{r}_\perp \cdot (W^{(0)} \hat{\boldsymbol{n}}_0) \right\} dl = \\ &2|\boldsymbol{a}_0|^2 \frac{\partial \psi_0}{\partial t} \int_\Gamma \boldsymbol{r}_\perp \cdot (W^{(0)\prime} \hat{\boldsymbol{n}}_0) \, dl \,. \end{aligned} \tag{3.53}$$

where we have used the symbol $\psi_0$ to indicate the particle angle determined at this order in the expansion. $W^{(0)\prime}$ is the scaled vorticity, defined as [cfr. (3.13d)]

$$W^{(0)\prime} = \frac{1}{2}\left[\boldsymbol{\nabla}_{\boldsymbol{y}} \boldsymbol{u}_1 - (\boldsymbol{\nabla}_{\boldsymbol{y}} \boldsymbol{u}_1)^T\right]. \tag{3.54}$$

Hence, the final form of the particle equation is

$$\kappa_0 \frac{\partial \psi_0}{\partial t} = -\xi_0^2 \mathcal{B} : (\boldsymbol{\nabla}_{\boldsymbol{x}} \boldsymbol{a}_0 \cdot \boldsymbol{\nabla}_{\boldsymbol{x}} \boldsymbol{a}_0) - \beta_1 \boldsymbol{q}^{(\kappa)} \cdot \boldsymbol{a}_0 - \chi_u P_{imlk} \epsilon_{il}^{(0)} \phi_{0,m} \phi_{0,k}, \tag{3.55}$$

where

$$\mathcal{B}_{ij} = \int_\Gamma \frac{1}{2}\left(\chi_{i,j} + \chi_{j,i} + \chi_{i,k}\chi_{j,k}\right)(\boldsymbol{r}_\perp \cdot \hat{\boldsymbol{n}}_0) \, dl, \tag{3.56a}$$

$$P_{imlk} = \int_\Gamma \left(\delta_{kl} + \frac{\partial R_l}{\partial y_k}\right)\left(\delta_{im} + \frac{\partial R_i}{\partial y_m}\right)(\boldsymbol{r}_\perp \cdot \hat{\boldsymbol{n}}_0) \, dl, \tag{3.56b}$$

$$\epsilon^{(0)} = \mathcal{I} + \alpha\mathcal{Q}^{(0)}, \tag{3.56c}$$

$$\boldsymbol{q}^{(\kappa)} = -\int_\Gamma \left[\kappa(\hat{\boldsymbol{n}}_0 \cdot \boldsymbol{r}_\perp)\mathcal{I} - 2\mathcal{W}\right] \boldsymbol{a}_S \, dl, \tag{3.56d}$$

$$\kappa_0 = \int_\Gamma \left[\boldsymbol{r}_\perp \cdot \left(\zeta' \mathcal{D}^{(0)\prime} \hat{\boldsymbol{n}}_0 - \hat{\boldsymbol{n}}_0 P_0\right)\right] dl + 2|\boldsymbol{a}_0|^2 \int_\Gamma \boldsymbol{r}_\perp \cdot \left(W^{(0)\prime} \hat{\boldsymbol{n}}_0\right) dl. \tag{3.56e}$$

To summarize, equations (3.40), (3.46) and (3.55) capture the macroscopic behavior of the system. Their coefficients are the key link between microscopic and macroscopic physics of the suspension. Normally, the homogenization procedure would stop here. However, in the specific case of liquid crystals a further simplification is possible, namely we can apply a second multiple scale expansion, this time in the time domain, to obtain a final set of macroscopic equations. We do this in the following section and then proceed to discuss in detail the physical meaning of the various terms in these equations.

**3.5. Multiple time scale analysis.** Looking at equations (3.40) and (3.55) we notice that $\xi_0^2$, $\chi_a$ and $\beta_1$ are extremely small parameters $\sim \mathcal{O}(10^{-7})$, see table 2.2. Away from defects the elastic and particle driving terms are small in comparison to the thermotropic terms. As a results when equations (3.40) and (3.55) are integrated to equilibrium, the dynamics in the absence of defects roughly correspond to a rapid equilibration of the scalar order parameter followed by a slow elastic reorientation. We now follow the method of [15] and use multiple scale analysis to obtain equations governing the slow elastic reorientation.

The slow reorientation dynamics are driven by terms of the order $\xi_0^2$. We simplify equations (3.40) by expanding in terms of $\eta_M = \xi_0^2$ and express $\beta_1 = \eta_M \hat{\beta}$, $\chi_a = \eta_M \hat{\chi}_a$, $\chi_u = \eta_M \hat{\chi}_u$ and $\frac{\partial}{\partial t} = \eta_M \frac{\partial}{\partial \hat{t}}$. We assume that all dynamics on a faster time-scale than $\hat{t}$ have reached equilibrium. Equation (3.55) is driven solely by terms of order $\eta_M$, its dynamics are confined solely to the slow elastic time-scale $\hat{t}$. The first order part of equation (3.40) is

$$\boldsymbol{a}_0 - \boldsymbol{a}_0 |\boldsymbol{a}_0|^2 = 0, \tag{3.57}$$

which defines an invariant manifold

$$|\boldsymbol{a}_0|^2 = 1. \tag{3.58}$$

At next order we find

$$\begin{aligned} &\boldsymbol{\nabla}_{\boldsymbol{x}} \cdot \mathcal{K} \boldsymbol{\nabla}_{\boldsymbol{x}} \boldsymbol{a}_0 + \hat{\chi}_a \left[ \boldsymbol{e}_M \left( 1 + 2 \frac{|\Omega_{\mathrm{np}}|}{|\Omega|} \right) + \boldsymbol{p} \right] \\ &\qquad + \frac{\hat{\beta}}{|\Omega|} \int_\Gamma (\boldsymbol{a}_S - \boldsymbol{a}_0)\, dl - \frac{\partial \boldsymbol{a}_0}{\partial \hat{t}} + \frac{2}{|\Omega|} \frac{\partial \psi_0}{\partial \hat{t}} \boldsymbol{a}_\perp = 4 \boldsymbol{a}_0 \left( \boldsymbol{a}_0 \cdot \boldsymbol{a}_1 \right). \end{aligned} \tag{3.59}$$

To obtain the time and space dependence of $\boldsymbol{a}_0$ we require that (3.59) posses a solution for any $\boldsymbol{a}_1$. The solvability condition is that the left hand-side of (3.59) is orthogonal to $\boldsymbol{a}_\perp = \mathcal{W} \boldsymbol{a}_0$: this ensures that both the left and right hand-side of (3.59) are in the direction of $\boldsymbol{a}_0$. Applying the solvability condition and re-expressing the result on the rapid time-scale we find

$$\begin{aligned} \boldsymbol{a}_\perp \cdot \frac{\partial \boldsymbol{a}_0}{\partial t} - \frac{2}{|\Omega|} \frac{\partial \psi_0}{\partial t} &= \xi_0^2 \left( \boldsymbol{\nabla}_{\boldsymbol{x}} \cdot \mathcal{K} \boldsymbol{\nabla}_{\boldsymbol{x}} \boldsymbol{a}_0 \right) \cdot \boldsymbol{a}_\perp \\ &\quad + \chi_a \left[ \boldsymbol{e}_M \left( 1 + 2 \frac{|\Omega_{\mathrm{np}}|}{|\Omega|} \right) + \boldsymbol{p} \right] \cdot \boldsymbol{a}_\perp + \frac{\beta_1}{|\Omega|} \left( \int_\Gamma \boldsymbol{a}_S\, dl \right) \cdot \boldsymbol{a}_\perp, \end{aligned} \tag{3.60a}$$

$$\boldsymbol{a}_0 \cdot \frac{\partial \boldsymbol{a}_0}{\partial t} = 0. \tag{3.60b}$$

These equations are valid for $\boldsymbol{x} \in \mathrm{D}_H$ and have boundary conditions (3.41). Equation (3.60a) is the solvability condition, while equation (3.60b) is obtained by differentiating (3.58). Together they define the dynamics of the nematic along the manifold of uniaxial $\mathcal{Q}$-tensors with scalar order parameter given by (3.57).

Equation (3.46), (3.55) and (3.60) are the final macroscopic equations for a two-dimensional suspension of freely rotating metallic particles in a nematic liquid crystal in the absence of defects.

The torque the particle experiences due to the elastic free energy is captured by $\mathcal{B}_{ij}$ in equation (3.55) and represents a screening effect. This term tends to align a particle so that it screens opposing boundary conditions. The surface interaction

with the nematic is captured by $\boldsymbol{q}^{(\kappa)}$ in equation (3.55) and favors aligning the particle easy axis with the macroscopic director. Its coefficient is the scaled anchoring energy coefficient $\beta_1$ rather than the unscaled value $\beta$: this is to reflect that the alignment equation is valid only in the weak anchoring limit discussed in section 3.1. The interaction with the electric field is determined by both the local field and the local alignment of the nematic. The term containing $P_{imlk}$ in equation (3.55) describes this coupling.

The terms in (3.60) offer a similar interpretation. In place of the screening effect we have an excluded volume effect given by $\mathcal{K}$. The surface interaction takes a slightly different form but still favors aligning the nematic with the local particle easy axis. The interaction with the electric field is split into two parts, the macroscopic field $\boldsymbol{e}_M$ and the polarization $\boldsymbol{p}$. The macroscopic field coupling is increased due to the volume occupied by metallic particles: the field is only non-zero outside the particles, but the total change in potential due to an externally driven field remains constant regardless of the presence of metallic particles. The polarization captures the additional field due to induced surface charges on the dopant particles.

**4. Numerical validation.** To check the accuracy of the macroscopic model derived in the previous section, we compare its predictions with numerical simulations of realistic, but numerically manageable, colloidal suspensions. This requires us to tackle two independent issues: the first is the integration of the cell problems, equations (3.19), (3.28) and (3.32), that define the parameters that appear in the macroscopic equations. Once these are known, the integration of the macroscopic equations (3.46), (3.55) and (3.60) is relatively trivial. The second is the integration of the microscopic equations (2.25), (2.29), (2.31) and (2.32). We discuss these two issues in turn and then compare the results of the two sets of simulations.

To use the macroscopic equations (3.46), (3.55), and (3.60) we must first solve the set of cell problems (3.19), (3.28) and (3.32) to obtain the effective material parameters. This can be accomplished using the finite element package COMSOL multiphysics (see section SM3 of the Supplementary materials for details). To integrate the macroscopic equations we use a spectral collocation method [47] to discretize in space and the MATLAB variable order solver ode15s, which uses implicit numerical differentiation, to integrate in time.

The macroscopic equations (3.46), (3.55), and (3.60) can be integrated with relative ease numerically in arbitrarily large macroscopic domains. However, for comparison with the microscopic equations (2.25), (2.29), (2.31), and (2.32) we select a one dimensional macroscopic domain, with $0 \leq x_2 \leq 1$. This is equivalent to a liquid crystal cell with flat surfaces at $x_2 = \{0, 1\}$ and uniform alignment conditions there. A potential difference $V$ is applied between $x_2 = 0$ and $x_2 = 1$. The equivalent microscopic system is a stack of up to 64 unit cells, each containing one particle, that is solved using a finite element method. The number of particles is large enough to make the model realistic, but small enough that the integration of the microscopic equations takes no more than a few hours on a high spec PC (as opposed to a few seconds for the macroscopic equations).

The microscopic equations (2.25), (2.29), (2.31), and (2.32) are solved in a microscopic domain consisting of a $1 \times N$ array of unit cells each containing a single identical particle. Within each cell the particle is free to rotate and equations (2.25), (2.29), (2.31) and (2.32) are solved throughout the whole system. The long sides of the array are subject to periodic boundary conditions while the ends are subject to appropriate Dirichlet conditions. In all cases we assume zero pre-tilt and constant

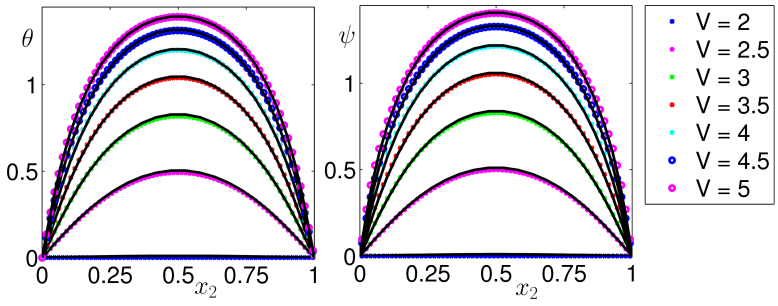


FIG. 4.1. *Director (left) and particle (right) angle as a function of distance into the cell for different values of the voltage applied to the cell. The solid lines are the solutions of the homogenized/macroscopic equations, while the colored points and circles are solutions of the microscopic equations computed using Comsol with $N = 64$ particles. Elliptic particles with semi-axes 0.1 and 0.23, the angle $\psi$ is formed by the semi-major axis and the $x_1$-axis and the anchoring energy is $\tilde{\mu} = 10^{-6}$ J $m^{-2}$.*

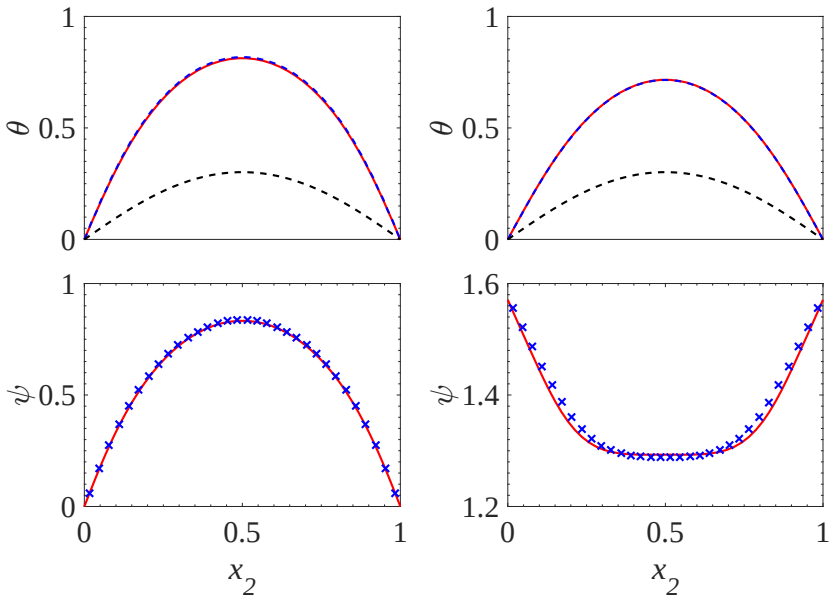


FIG. 4.2. *Director (top) and particle (bottom) angle as a function of distance into the cell at $V = 3$ for $\tilde{\mu} = 10^{-6}$ $Jm^{-2}$ (left) and $\tilde{\mu} = 3.1 \cdot 10^{-8}$ $Jm^{-2}$ (right). In all plots the red solid lines are the result of the homogenized/macroscopic equations, while the blue dashed lines and crosses are the solutions of the microscopic equations for $N = 32$ elliptic particles of the same size as in figure 4.1. In the stronger anchoring case (left column) the particles are slaved to the director field and $\theta$ and $\psi$ have the same profile. In the weaker anchoring case (right column) the particles partially detach from the liquid crystal and align with the electric field. The black dashed line in the top two graphs is the director angle in the case of a pure liquid crystal.*

potential across the ends of the stack. Equation (2.25) is implemented as a general form PDE, the electrostatics package is used to compute the electric field, the particles motion is included as a set of global ODEs.

A comparison between the homogenized equations and the large-scale finite element simulations is shown in figure 4.1 for a range of voltages $V = 2$ to $V = 5$ applied

to a suspension of elliptical particles. For each voltage 64 particles were used in the microscopic simulations. There is excellent agreement at all voltages.

Figure 4.2 illustrates the effect of the anchoring energy on the alignment of the liquid crystal (top graphs) and of the particles (bottom graphs) in response to an electric field parallel to the $x_2$ axis. The red lines represent the results of the macroscopic model, while the blue dashed lines and crosses are the solution of the microscopic equations with $N = 32$ elliptic particles of the same size as in figure 4.1. This figure shows once again that the agreement between microscopic and macroscopic models is remarkably good, even at relatively large values of $\eta$: the microscopic model simulated in this figure has $N = 32$ particles which corresponds to $\eta = 1/32$. The figure also illustrates very clearly the effect of microscopic parameters on the system behavior: for stronger anchoring (left column) the liquid crystal and the particles are slaved to each other and $\theta(x_2)$ and $\psi(x_2)$ have the same profile. For weaker anchoring (right column) the particles are approximately parallel to the electric field $\psi \approx \pi/2$ across the entire cell, while the director profile is still far from saturation: the particles are influenced more by the applied field and screening effects, both of which favor $\psi = \pi/2$, than by the surface anchoring. For comparison, the black dashed lines in the top panels of figure 4.2 are the alignment of the liquid crystal in the absence of particles: the amplitude of the director deflection is much smaller, indicating clearly how the particles amplify the response of the liquid crystal to external fields. Finally, we have checked that the particle symmetry does not affect the quality of the approximation (see section SM4 of the Supplementary material).

**5. Discussion.** In this paper we studied the alignment of a nematic liquid crystal containing freely rotating metallic particles using the method of asymptotic homogenization. We have derived a set of macroscopic equations that include the shape and composition of the dopant particles directly. We have shown that the model developed here agrees well with large-scale numerical simulations. The main difference between the theory developed here and that developed previously [6] is the presence of particle dynamics. We find that the particles are aligned by elastic screening interactions with the liquid crystal, surface anchoring effects and a direct interaction with the electric field. As in previous work [6] the key advantage of using homogenization is the ability to link the macroscopic quantities such as susceptibilities, to the micro-structure of the problem.

The main assumption we have made in deriving our model is that a separation of scales exists between the inter-particle spacing and the macroscopic size of the system. This is a valid assumption for low concentration colloids that are typically studied experimentally. One consequence of this assumption is that the alignment cannot vary significantly within the neighborhood of a particle. This precludes the study of defects. In addition we have assumed that the anchoring energy density is scaled with the concentration of particles in the system. This has some impact on the range of systems that may be modeled. Our model is certainly valid for anchoring energies of the order of $10^{-6}$ $\mathrm{Jm}^{-2}$ (see figure 4.2). Preliminary work has shown that if the weak anchoring constraint is dropped we obtain both an additional set of cell problems which couple the elastic and surface interactions and terms quadratic in the anchoring strength $\tilde{\mu}$ in the macroscopic equations. This will be explored further in future work.

Future work may explore extending this theory to the three dimensional case, incorporating fluid flow more completely and allowing for more general particle motion. The extension to three dimensions does not introduce any new physics to this

problem, but requires considerably longer algebra as the $\mathcal{Q}$-tensor has 5 independent components and the particle orientation is described by two angles. Moreover, the computational time needed to solve the cell problems and verify the model against large-scale numerical simulations will increase significantly. Incorporating the full dissipation function derived by Sonnet *et al.* [44] would couple the particle and nematic dynamics leading to a more complicated model. It may be possible to incorporate translating particles using the method employed by Richardson and Chapman [37]. This method involves making a change of coordinates that maps a seemingly non-periodic problem into a periodic problem in general curvilinear coordinates. Treating moving particles in this way may allow the particles to move away from the lattice configuration we are currently confined to.

In principle it may be possible to extend this work to the strong anchoring case. As strong anchoring is essential for self-assembly this is certainly a problem well worth studying. However, it is non-trivial and would require a considerable recasting of the homogenization procedure: one of the key consequences of the weak anchoring limit is that the lowest order director field $\boldsymbol{a}_0$ is a function of the macroscopic coordinates only. This would be no longer the case if defects were present.

**6. Conclusions.** Despite a number of assumptions, the theory developed in this paper represents an important step forward in modeling the interactions of a liquid crystal with small particles. The use of homogenization ties the average properties of the liquid crystal to the dopant material properties, size, density and shape. This approach opens up the possibility of using optimization to design particles for a specific application without the need for large scale simulation and lays the groundwork for future model development.

**Acknowledgments.** The authors thank Prof Malgosia Kaczmarek and Prof Tim Sluckin for helpful discussions.

## REFERENCES

[1] R. Alexandre, *Homogenisation and $\theta - 2$ convergence*, Proceedings of the Royal Society of Edinburgh: Section A Mathematics, 127 (1997), pp. 441–455, http://dx.doi.org/10.1017/S0308210500029863.

[2] G. Allaire, *Homogenization and two-scale convergence*, SIAM Journal on Mathematical Analysis, 23 (1992), pp. 1482–1518.

[3] T. Araki and H. Tanaka, *Surface-sensitive particle selection by driving particles in a nematic solvent*, J. Phys.: Condens. Matter, 18 (2006), pp. L193–L203, http://dx.doi.org/10.1088/0953-8984/18/15/L05.

[4] R. Barberi, F. Ciuchi, G. E. Durand, M. Iovane, D. Sikharulidze, A. M. Sonnet, and E. G. Virga, *Electric field induced order reconstructionin a nematic cell*, Eur. Phys. J. E, 13 (2004), pp. 61–71, http://dx.doi.org/10.1140/epje/e2004-00040-5.

[5] A. G. Belyaev, A. L. Pyatnitskiĭ, and G. A. Chechkin, *Asymptotic behavior of a solution to a boundary value problem in a perforated domain with oscillating boundary*, Siberian Math. J., 39 (1998), pp. 621–644, http://dx.doi.org/10.1007/BF02673049.

[6] T. P. Bennett, G. D'Alessandro, and K. R. Daly, *Multiscale models of colloidal dispersion of particles in nematic liquid crystals*, Phys. Rev. E, 90 (2014), p. 062505, http://dx.doi.org/10.1103/PhysRevE.90.062505.

[7] M. Briane, *Three models of non periodic fibrous materials obtained by homogenization*, RAIRO-Modél. Math. Anal. Numér., 27 (1993), pp. 759–775.

[8] M. Briane, *Homogenization of a non-periodic material*, J. Math. Pures Appl., 73 (1994), pp. 47–66.

[9] M. Bruna and S. J. Chapman, *Diffusion in spatially varying porous media*, SIAM Journal on Applied Mathematics, 75 (2015), pp. 1648–1674, http://dx.doi.org/10.1137/141001834.

[10] S. V. Burylov and Y. L. Raikher, *Macroscopic Properties of Ferronematics Caused by Orientational Interactions on the Particle Surfaces. I. Extended Continuum Model*, Mol. Cryst.

Liq. Cryst., 258 (1995), pp. 107–122, http://dx.doi.org/10.1080/10587259508034552.
[11] S. V. Burylov and Y. L. Raikher, *Macroscopic Properties of Ferronematics Caused by Orientational Interactions on the Particle Surfaces. II. Behavior of Real Ferronematics in External Fields*, Mol. Cryst. Liq. Cryst., 258 (1995), pp. 123–141, http://dx.doi.org/10.1080/10587259508034553.
[12] M. G. Campbell, M. Tasinkevych, and I. I. Smalyukh, *Topological polymer dispersed liquid crystals with bulk nematic defect lines pinned to handlebody surfaces*, Phys. Rev. Lett., 112 (2014), p. 197801, http://dx.doi.org/10.1103/PhysRevLett.112.197801.
[13] S. Chapman and S. McBurnie, *Integral constraints in multiple-scales problems*, Eur. J. Appl Math., 26 (2015), p. 595614, http://dx.doi.org/10.1017/S0956792514000412.
[14] G. A. Chechkin and A. L. Piatnitski, *Homogenization of boundary-value problem in a locally periodic perforated domain*, Appl. Anal., 71 (1998), pp. 215–235, http://dx.doi.org/10.1080/00036819908840714.
[15] K. R. Daly, G. D'Alessandro, and M. Kaczmarek, *An Efficient Q-Tensor-Based Algorithm for Liquid Crystal Alignment away from Defects*, SIAM J. Appl. Math., 70 (2010), pp. 2844–2860, http://dx.doi.org/10.1137/100796467.
[16] P. G. de Gennes, *The Physics of Liquid Crystals*, Clarendon press Oxford, 1974.
[17] J. Dontabhaktuni, M. Ravnik, and S. Žumer, *Quasicrystalline tilings with nematic colloidal platelets*, Proc. Natl. Acad. Sci. USA, 111 (2014), pp. 2464–2469, http://dx.doi.org/10.1073/pnas.1312670111.
[18] D. F. Gardner, J. S. Evans, and I. I. Smalyukh, *Towards reconfigurable optical metamaterials: Colloidal nanoparticle self-assembly and self-alignment in liquid crystals*, Mol. Cryst. Liq. Cryst., 545 (2011), pp. 3/[1227]–21/[1245], http://dx.doi.org/10.1080/15421406.2011.571966.
[19] E. C. Gartland, P. Palffy-Muhoray, and R. S. Varga, *Numerical minimization of the landau-de gennes free energy: Defects in cylindrical capillaries*, Mol. Cryst. Liq. Cryst., 199 (1991), pp. 429–452, http://dx.doi.org/10.1080/00268949108030952.
[20] M. A. Gharbi, D. Sec, T. Lopez-Leon, M. Nobili, M. Ravnik, S. Zumer, and C. Blanc, *Microparticles confined to a nematic liquid crystal shell*, Soft Matter, 9 (2013), pp. 6911–6920, http://dx.doi.org/10.1039/C3SM00126A.
[21] T. Hegmann, H. Qi, B. Kinkead, V. Marx, H. Girgis, and P. Heiney, *Functionalized metal and semiconductor nanaporticle doped liquid crystals – Modifying optical and electro-optical properties*, Can. Metallurgical Quat., 48 (2009), pp. 1–10.
[22] T. Hegmann, H. Qi, and V. Marx, *Nanoparticles in Liquid Crystals: Synthesis, Self-Assembly, Defect Formation and Potential Applications*, J. Inorg. Organomet. Polym. Mater., 17 (2007), pp. 483–508, http://dx.doi.org/10.1007/s10904-007-9140-5. 10.1007/s10904-007-9140-5.
[23] U. Hornung, *Homogenization and Porous Media*, Springer, 1996.
[24] I. C. Khoo, D. H. Werner, X. Liang, , and A. Diaz, *Nanosphere dispersed liquid crystals for tunable negative?zero?positive index of refraction in the optical and terahertz regimes*, Opt. Lett., 31 (2006), pp. 2592–2594.
[25] O. Kurochkin, Y. K. Murugesan, T. Bennett, G. D'Alessandro, Y. Reznikov, B. Tang, G. H. Mehl, and M. Kaczmarek, *Thermal optical non-linearity of nematic mesophase enhanced by gold nanoparticles - an experimental and numerical investigation*, Phys. Chem. Chem. Phys., 18 (2016), pp. 11503–11512, http://dx.doi.org/10.1039/C6CP00116E.
[26] L. M. Lopatina and J. V. Selinger, *Theory of Ferroelectric Nanoparticles in Nematic Liquid Crystals*, Phys. Rev. Lett., 102 (2009), p. 197802, http://dx.doi.org/10.1103/PhysRevLett.102.197802.
[27] M. Mascarenhas and D. Poliševski, *The warping, the torsion and the Neumann problems in a quasi-periodically perforated domain*, RAIRO-Modél. Math. Anal. Numér., 28 (1994), pp. 37–57.
[28] T. Miyama, J. Thisayukta, H. Shiraki, Y. Sakai, Y. Shiraishi, N. Toshima, and S. Kobayashi, *Fast Switching of Frequency Modulation Twisted Nematic Liquid Crystal Display Fabricated by Doping Nanoparticles and Its Mechanism*, Jpn. J. Appl. Phys., 43 (2004), pp. 2580–2584, http://dx.doi.org/10.1143/JJAP.43.2580.
[29] A. Muntean and T. L. Van Noorden, *Corrector estimates for the homogenization of a locally periodic medium with areas of low and high diffusivity*, Eur. J. Appl Math., 24 (2013), pp. 657–677, http://dx.doi.org/10.1017/S0956792513000090.
[30] I. Muševič, M. Škarabot, U. Tkalec, M. Ravnik, and S. Žumer, *Two-dimensional nematic colloidal crystals self-assembled by topological defects*, Science, 313 (2006), pp. 954–958, http://dx.doi.org/10.1126/science.1129660.
[31] G. Nguetseng, *A general convergence result for a functional related to the theory of homoge-*

*nization*, SIAM Journal on Mathematical Analysis, 20 (1989), pp. 608–623.
[32] E. Ouskova, D. Lysenko, S. Ksondzyk, L. Cseh, G. H. Mehl, V. Reshetnyak, and Y. Reznikov, *Strong cubic optical nonlinearity of gold nanoparticles suspension in nematic liquid crystal*, Mol. Cryst. Liq. Cryst., 545 (2011), pp. 123/[1347]–132/[1356], http://dx.doi.org/10.1080/15421406.2011.568883.
[33] G. Pavliotis and A. Stuart, *Multiscale methods: averaging and homogenization*, Springer-Verlag, New York, 1 ed., 2007.
[34] S. K. Prasad, K. L. Sandhya, G. G. Nair, U. S. Hiremath, C. V. Yelamaggad, and S. Sampath, *Electrical conductivity and dielectric constant measurements of liquid crystal-gold nanoparticle composites*, Liq. Cryst., 33 (2006), pp. 1121–1125, http://dx.doi.org/10.1080/02678290600930980.
[35] M. Ptashnyk, *Two-scale convergence for locally periodic microstructures and homogenization of plywood structures*, Multiscale Model. Simul., 11 (2013), pp. 92–117, http://dx.doi.org/10.1137/120862338.
[36] H. Qi, B. Kinkead, and T. Hegmann, *Unprecedented Dual Alignment Mode and Freedericksz Transition in Planar Nematic Liquid Crystal Cells Doped with Gold Nanoclusters*, Adv. Funct. Mater., 18 (2008), pp. 212–221, http://dx.doi.org/10.1002/adfm.200701327.
[37] G. Richardson and S. J. Chapman, *Derivation of the bidomain equations for a beating heart with a general microstructure*, SIAM Journal on Applied Mathematics, 71 (2011), pp. 657–675, http://dx.doi.org/10.1137/090777165.
[38] G. Richardson, G. Denuault, and C. P. Please, *Multiscale modelling and analysis of lithium-ion battery charge and discharge*, Journal of Engineering Mathematics, 72 (2011), pp. 41–72, http://dx.doi.org/10.1007/s10665-011-9461-9.
[39] R. W. Ruhwandl and E. M. Terentjev, *Monte Carlo simulation of topological defects in the nematic liquid crystal matrix around a spherical colloid particle*, Phys. Rev. E, 56 (1997), pp. 5561–5565, http://dx.doi.org/10.1103/PhysRevE.56.5561.
[40] B. Senyuk, Q. Liu, S. He, R. D. Kamien, R. B. Kusner, T. C. Lubensky, and I. I. Smalyukh, *Topological colloids*, Nature, 493 (2013), pp. 200–205, http://dx.doi.org/10.1038/nature11710. 10.1038/nature11710.
[41] B. Senyuk, M. B. Pandey, Q. Liu, M. Tasinkevych, and I. I. Smalyukh, *Colloidal spirals in nematic liquid crystals*, Soft Matter, 11 (2015), pp. 8758–8767, http://dx.doi.org/10.1039/C5SM01539A.
[42] S. M. Shelestiuk, V. Y. Reshetnyak, and T. J. Sluckin, *Frederiks transition in ferroelectric liquid-crystal nanosuspensions*, Phys. Rev. E, 83 (2011), p. 041705, http://dx.doi.org/10.1103/PhysRevE.83.041705.
[43] S. Shkoller, *An approximate homogenization scheme for nonperiodic materials*, Comput. Math. Appl., 33 (1997), pp. 15 – 34, http://dx.doi.org/10.1016/S0898-1221(97)00003-5.
[44] A. Sonnet, P. Maffettone, and E. Virga, *Continuum theory for nematic liquid crystals with tensorial order*, J. Non-Newtonian Fluid Mech., 119 (2004), pp. 51 – 59, http://dx.doi.org/10.1016/j.jnnfm.2003.02.001.
[45] A. M. Sonnet and E. G. Virga, *Dissipative ordered fluids: Theories for liquid crystals*, Springer, New York, 1st ed., 2012.
[46] H. Stark, *Director field configurations around a spherical particle in a nematic liquid crystal*, Eur. Phys. J. B, 10 (1999), pp. 311–321, http://dx.doi.org/10.1007/s100510050860.
[47] L. N. Trefethen, *Spectral Methods in Matlab*, SIAM, Philadelphia, 2000.
[48] L. Zadoina, B. Lonetti, K. Soulantica, A.-F. Mingotaud, M. Respaud, B. Chaudretc, and M. Mauzac, *Liquid crystalline magnetic materials*, J. Mat. Chem., 19 (2009), pp. 8075–8078, http://dx.doi.org/10.1039/B915075G.
[49] Q. Zhang, P. J. Ackerman, Q. Liu, and I. I. Smalyukh, *Ferromagnetic switching of knotted vector fields in liquid crystal colloids*, Phys. Rev. Lett., 115 (2015), p. 097802, http://dx.doi.org/10.1103/PhysRevLett.115.097802.